buildings

MDPI

Article

Acoustic Ambience and Simulation of the Bullring of Ronda (Spain)

Manuel Martín-Castizo [1,*], Sara Girón [2] and Miguel Galindo [2]

[1] Escuela Técnica Superior de Arquitectura, Universidad de Sevilla, Avda. Reina Mercedes 2, 41012 Sevilla, Spain
[2] Instituto Universitario de Arquitectura y Ciencias de la Construcción (IUACC), Departamento de Física Aplicada II, Universidad de Sevilla, Avda. Reina Mercedes 2, 41012 Sevilla, Spain; sgiron@us.es (S.G.); mgalindo@us.es (M.G.)
* Correspondence: manmarcas1@alum.us.es

Abstract: The bullring of Ronda, one of the oldest in Spain, declared in 1993 as an Asset of Cultural Interest, occupies a paramount place among the buildings of its type thanks to its outstanding beauty. Its configuration as an open-air enclosure with a circular floor plan, as an evocation of the ancient Roman amphitheaters, and its interior with galleries on two levels that house the audience play a fundamental role in the acoustic energy decay and diffusion of the space. The link between architecture and acoustics of the Ronda bullring has been carried out by using on-site measurements and simulation techniques. To this end, an acoustic model is created, which is adjusted by taking the set of 3D impulse responses recorded on-site. The presence of the public and the various sound sources that exist during the bullfight itself are analyzed in the simulations, whereby the conditions of occupation and vacancy are compared, as are the variations due to the location of the sources. Finally, speech intelligibility conditions are simulated with a human directivity source. The precision of the virtual acoustic model enables the sound architecture of this singular space to be ascertained and preserved, thereby incorporating sound as an associated intangible heritage.

Keywords: acoustics of bullrings; heritage acoustics; acoustic simulation; digital models

Citation: Martín-Castizo, M.; Girón, S.; Galindo, M. Acoustic Ambience and Simulation of the Bullring of Ronda (Spain). *Buildings* **2024**, *14*, 298. https://doi.org/10.3390/buildings14010298

Academic Editor: Ángel Fermín Ramos Ridao

Received: 13 December 2023
Revised: 15 January 2024
Accepted: 19 January 2024
Published: 22 January 2024

1. Introduction and Goals

Bullfighting is an event of profound importance in Spanish life, which has implications for many social, economic, cultural, and artistic activities. It is not in vain that Spanish legislation recognizes bullfighting as an essential part of Spain's historical, artistic, cultural, and ethnographic heritage. The bullring, as a space where bullfighting takes place, is a construction that "combines its historical and architectural value with the virtue of being a meeting place, public space and celebration scene, and a building closely linked to the social and urban fabric of the city in which it is located" [1]. This article continues the research on the acoustics of bullrings that the authors have been developing with the general objective of contributing to the narrative of bullfighting through the link between architecture and the sounds of voice, atmosphere, effects, music, and silence that are manifested in bullrings [2], thus providing valuable information regarding its renowned architectural heritage.

In the listening process, the acoustic space in which the acoustic source and receiver are immersed is decisive. Each space has its own architecture of sound. The principles and foundations of aural architecture as the aural perception of space were laid out by Blesser and Salter [3]. The aural architecture of a space is determined by its physical attributes (its geometry, its delimiting surfaces, and the objects that it contains) and by the cultural context. When listeners share similar sensations immersed in the same aural architecture, they become a relatively homogeneous group. Hearing, along with its active complement, listening, is a means by which humans perceive life events, visualize spatial geometry aurally, experience social relationships, and retain a memory of experiences.

Sounds that listeners perceive in certain spaces and places constitute vestiges of our collective memory and form part of that intangible cultural heritage that is worth studying and preserving for the understanding of culture and society [4,5]. The viability of adapting acoustic theory and methods to archaeology enables the archaeological interpretation of ancient places and materials to be extended and their re-sounding to be carried out [6–8].

The acoustics of prominent historical-cultural buildings have received substantial attention in recent decades thanks to precise measurements that contribute significantly towards ascertaining, preserving, and disseminating their acoustic heritage [9–11]. The complete description of the spatial propagation of sound is obtained from the 3D impulse response by analyzing the distribution of sound energy in the time-frequency and spatiotemporal domains, whereby sources and receivers are placed in the relevant positions.

The safeguarding of acoustic heritage was promoted by Gerzon [12] through the systematic collection of 3D impulse response measurements in order to evaluate the behavior of unique buildings and to preserve them for posterity. These 3D impulse response measurement systems using compact microphone arrays have been under development since the late 1980s [13–18], of which the recent research by the Lokki group [19] deserves mention.

Likewise, Beranek [20] defined texture as the "subjective impression that listeners derive from the patterns in which the sequence of early sound reflections arrive at their ears", referring to early reflections as the acoustic signature [21] of any venue. The author was referring to that characteristic of rooms whose early reflections should not be too far apart nor too stacked. Recent research addresses the possible relationship between the reflection sequence and the acoustic signature of a room [19,21,22] and can affirm that early reflections provide a sound representation of its architectural form.

On the other hand, digital acoustic simulations have been under development for the last 60 years [23–25]. The acoustic simulation methods of venues can be classified into two groups: one based on solving the wave equation numerically and another based on the approximation by means of rays or geometric acoustics (GA) [26]. The choice of the most appropriate method is influenced by factors such as the physical size of the room, the frequency range of interest, the accuracy required, and the computing resources available. The applications of the wave-based methods are limited to low-medium frequencies and small rooms, while the GA methods, based on the validity and application of the laws of specular and diffuse reflection, offer better results in large rooms and at relatively high frequencies where wave phenomena are less significant. Currently, hybrid algorithms that provide accurate broadband results by taking advantage of the benefits and minimizing the drawbacks of each method are emerging [23,27].

The acoustic simulations of heritage spaces enable the knowledge thereof to be revealed and their sound architecture to be preserved [28–32], given that the quality of the documentary and graphic information employed to create the model determines the accuracy of the prediction. In digital acoustic modeling, the details are simplified to improve the approximation; when studying the acoustics of historical-cultural buildings, however, the effect of architectural detail can prove to be of major importance [10].

To ensure that the virtual model resembles reality, a calibration is carried out by comparing the acoustic behavior of the model with that of the building itself, obtained through acoustic measurements in situ. The criteria adopted for a correct validation should consider the estimation of the uncertainty of the values measured in situ and the sources of uncertainty of commercial software [33,34]. In open-air and unroofed venues, as in the case of bullrings, the opening to the sky often dominates the architecture, which causes problems in the calibration of their models. Certain room simulations, with high absorption in ceilings and reflective walls, generate an unrealistic lengthening of their reverberation time [35,36], which leads us to consider it necessary to modify the absorption coefficient therein.

The objective of this work is to present the integral characterization of the sound field of the bullring of Ronda based on the parametric acoustic description and the spatiotemporal and spectro-temporal analysis of the 3D impulse responses measured in the space in the absence of an audience. The study considers the positions of the sound sources

involved in the bullfighting spectacle. It is completed with the results of a computational acoustic model validated with the experimental measurements to extend the analysis to include the presence of the public in the bullring.

This paper is organized as follows: subsequent to this introduction; the Section 2 corresponds to a brief history and architectural description of the building under study; the Section 3 exposes the materials and methods; the Sections 4 and 5 state the results obtained in the empirical campaign and in the digital simulations and their discussions, respectively. Finally, the Section 6 summarizes the main conclusions of this study.

2. The Real Maestranza de Caballería de Ronda and Its Bullring

The Real Maestranza de Caballería de Ronda (RMCR), created in the 16th century as a noble corporation for the defense of the city and its territory, is today a non-profit charity dedicated to the conservation, dissemination, and research of its historical and documentary heritage, to the promotion of culture, and to the teaching of horse riding [37]. Among its properties, the bullring, located within the historical center of Ronda, is one of the oldest bullrings in Spain, takes pride of place, and was declared an Asset of Cultural Interest in the monument category in 1993.

2.1. Brief History of the Bullring

The city of Ronda is located in the south of Spain in a unique natural setting: a lofty rocky promontory bordered by sheer cliffs. This exceptional orography has led to its military defensive character and has conditioned its urban development. The constrained limits of the old city gave rise to a new neighborhood outside the walls on the other side of the Guadalevin River. The construction of the New Bridge (1759–1787) by the architect José Martín de Aldehuela over the rocky gorge of the Tagus enabled the urban development of Ronda in a high, flat, sunny, and wide place.

Ronda had its appropriate places where equestrian games and bullfighting took place [38,39]. Unlike other Spanish cities with a bullfighting tradition (such as Seville, Madrid, Córdoba, and Granada), in Ronda the scenario of the festival jumped directly from the Plaza Mayor to the Plaza de Toros built for this purpose, situated outside the urban area, and constructed on the Hollanquilla plain, without going through the stage of using provisional bullrings built of wood, as experienced elsewhere.

In the second half of the 18th century, Neoclassicism became the prevailing style, with the Roman amphitheaters as an example of the best archetype and antecedent for an outdoor performance. The circular shape, leaving behind the quadrangular space that was characteristic of its equestrian exhibitions, is an example of the RMCR promoting bullfighting on foot. Since its official inauguration in 1785, numerous interventions have been carried out on the building, such as the transfer of the main doorway to its current location, the work due to the destructive aftermath of subsequent wars, and deterioration caused by the passage of time. In recent years, the RMCR has followed a major conservation and maintenance program for the recovery and improvement of the bullring.

With regard to bullfighting, during the 19th and 20th centuries, the world's best bullfighters performed here since the bullring of the Maestranza of Ronda remained a sign of glory as the cathedra and historical center of bullfighting.

2.2. Architectural and Constructive Description of the Bullring

The bullring of the Royal Maestranza in Ronda occupies a prime place among buildings of its type due to its outstanding beauty. Circular in shape, as an evocation of the ancient Roman amphitheaters, it responds to the aesthetics of the Neoclassical style typical of the 18th century [40,41]. The floor plan is arranged according to the logic of its use and construction, where the axis defined by the main gate is a principal feature, formerly aligned with the new path of urban growth that would later become the New Bridge and the bullpen. Another axis, orthogonal to that previous, marks the door for the crews and dragging mules.

Its interior façade has two floors with continuous galleries, reminiscent of the double-arched balcony of the Collegiate Church of Santa María located in the Plaza Mayor, which had been used as a platform for equestrian shows. The double gallery of arcades has 136 columns forming 68 inset arches on their fronts and is supported by Tuscan columns on a plinth finished off at the top with flamingos that protrude from the roof. The four arches corresponding to the axes are somewhat larger than the rest, whereby the arch of the main or Royal box is formed of two fluted drum columns upon which an arch decorated with plant motifs rests. The grandstands are distributed across both galleries, with five rows of stands each (Figure 1a).

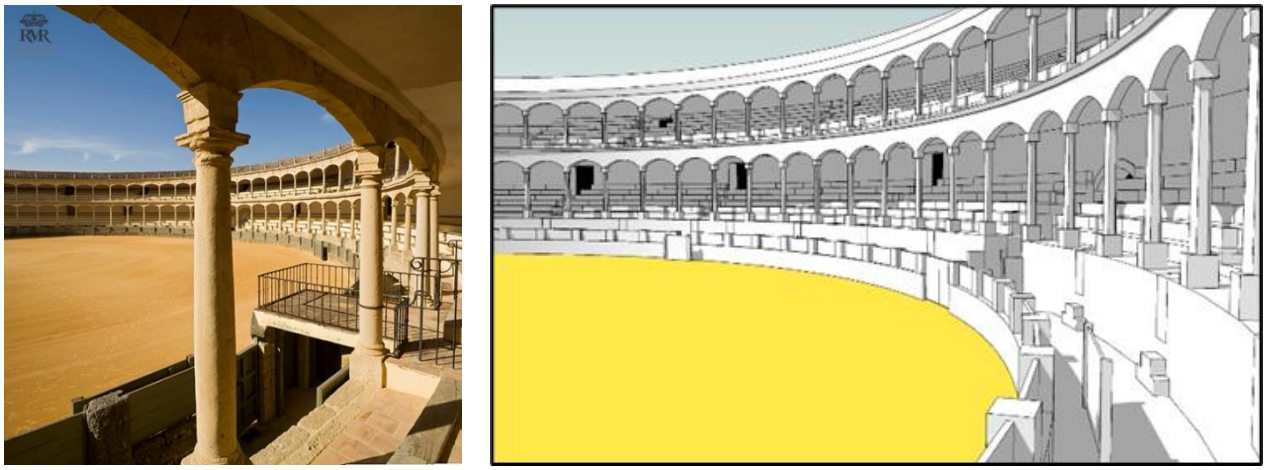

(**a**) (**b**)

Figure 1. (**a**) General view of the interior of the RMCR Bullring. (Source: RMCR). (**b**) Simplified 3D model of the interior of the bullring.

The building rises through a structure of three concentric rings. The outer ring and the middle ring are stone walls with mud and lime mortar, while the inner ring, with a diameter of 64.45 m, is made up of a double gallery of arcades. The spaces between these rings are used for access, warehouses, and outbuildings.

The double arches are built in yellowish sandstone extracted from the quarries near Ronda, which gives the bullring its distinguishing hallmark. The exterior of the bullring shows smooth, whitewashed walls where some holes have been inserted. The gabled roof, protected with Arab tiles, is supported by a framework of fir wood, a singular and unique species from the Ronda mountains.

The arena is one of the largest that exists, with a diameter of 60 m. The albero sand that covers it provides a peculiar, unique, and different canvas. Albero is a calcarenite, a sedimentary rock of materials of marine origin with a characteristic ochre color, which is extracted from a Sevillian region. The barrier in the arena is built of stone and wood and was later erected in line with the bullpen door. Access from the circular passageway is through four doors located in the center of each of the zones into which the bullring is divided by the two main axes. The circular passageway to the stands could be accessed through several cuts in the stone, which is covered with wood today and was used in ancient times for public access to the arena.

3. Materials and Methods

This study has been carried out inside the RMCR bullring. Its configuration as an open-air space and the fact that bullfights are performances in which the spoken word, music, and silence all play their role, making it especially interesting from an acoustic point of view.

3.1. Graphic Documentation and 3D Geometric Modelling

The 3D geometric models are prepared by using Sketchup Pro [42] modeling software from the graphic documentation and planimetry provided by the architects of the RMCR bullring [43] and from the photographs obtained in situ. To facilitate the export of the models created in Sketchup to the acoustic simulation program ODEON [44], the SU2Odeon plugin is available, which permits the export of complicated models and of sources and receivers, thereby positioning them directly in the Sketchup model.

In the context linked to research, dissemination, and preservation of cultural heritage, a much more detailed and rigorous first model can be created. From this first detailed model, another more simplified model used in the acoustic simulation is made, whereby all those elements and surfaces that do not necessarily translate into a higher precision of the simulated results are eliminated [26]. In particular, the acoustic model of the RMCR bullring, with a volume of 69,237 m^3, 15,749 surfaces, and a total interior area of 18,843 m^2, has been created by smoothing columns, cornices, and pilasters and by eliminating the wooden framework, pinnacles, etc. As good practice, the model surfaces were labeled to correspond to a specific material in the simulation stage (Figure 1b). The current capacity of the bullring is approximately 4890 spectators.

3.2. Sound Sources, Segments, and Audience Positions

During the bullfight itself, the silence of its protagonists predominates but is interspersed, both with voices and with music. The voices are between the bullfighters and their assistants, picadors and banderilleros, with the people of the passageway, even with the public present, and include the irrational dialogue between bullfighter and bull. The music emerges in two manifestations: the bugle calls to signal the changes of the third phase of the bullfight and the pasodoble interpretations in the repertoire of the music band that performs in the bullrings. The public can also show their appreciation with applause and ovations or, in contrast, with whistles and cries of censorship. Following the guide published by the authors to perform acoustic measurements in circular bullrings, and in accordance with the characteristics of bullfighting, four source positions are proposed in this bullring [2].

The first position (S1) in the center of the arena is considered a reference due to its central symmetry and equidistance to all points in the bullring. The second position (S2) is chosen in the segment of the ring where most of the bullfighting takes place. Specifically, it is located at the intersection of the 7 m picador line (double circular line drawn in the sand to mark the ground where the bulls are pitted) with the axis indicated by the old main gate and the bullpen gate. The third position (S3) is in a central place in the box reserved for the music band. The fourth position (S4) is in the lower grandstands, a position occupied by the audience that characterizes the ambient sound of the spectators.

For the location of the receiving positions, the disposition of the spectators around the arena is considered. The central symmetry of the bullring enables all the receiving positions to be located in only one-half of the enclosure. The exact location of the receiving positions is set at the intersections of some of the 12 reference radii with the barrier of the passageway or the rows of the grandstands. The direction defined by the 12 o'clock radius is made to coincide with the geographic North. Under the above conditions, 12 receivers are chosen in the positions of 2 in the barrier of the passageway and 5 in the lower grandstand, row no. 3; and 5 in the upper grandstand, row no. 3; as shown in Figure 2a,b.

The multi-source scenario in which the bullfighting event takes place makes it advisable to employ a good number of source-receiver combinations to understand its sound field. Table 1 shows the 48 source-receiver combinations that have been registered: those combinations that lack direct sound often depend on the positions of the sources in grandstands when said sources are not in the spectators' line of sight.

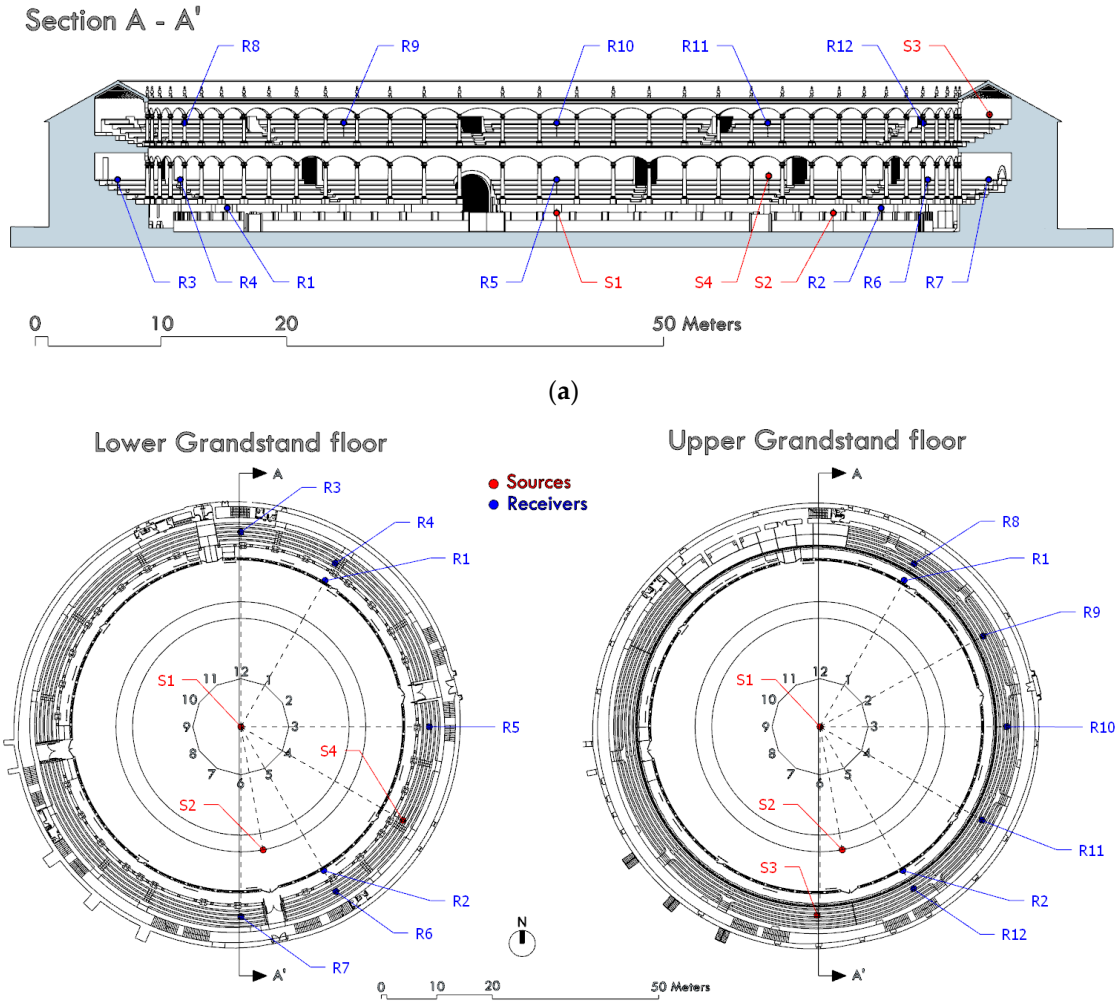

Figure 2. (**a**) Section and (**b**) floor plans of the bullring of Ronda showing the source and receiver positions.

Table 1. Source-receiver combinations. (o) Receivers with direct sound. (x) Receivers without direct sound.

		Receivers											
		R1	**R2**	**R3**	**R4**	**R5**	**R6**	**R7**	**R8**	**R9**	**R10**	**R11**	**R12**
Sources	S1	o	o	o	o	o	o	o	o	x	o	o	o
	S2	o	o	o	o	o	o	o	o	o	x	o	o
	S3	o	x	o	o	o	x	x	o	x	o	o	o
	S4	o	o	o	o	o	o	o	o	o	x	x	x

3.3. Experimental Measurements

The acoustic experimental measurements were carried out without the presence of the public by following the protocol established in the ISO 3382 standard [45,46]. Environmental conditions were monitored by means of measuring the temperature with ±1 °C of accuracy; the variation of temperature during the days of measurement ranged from 26.3 °C to 33.2 °C, and relative humidity was taken with an accuracy of ±5% with a range of variation from 34.8% to 49.0%. There was no wind during measuring times (air velocity less than 0.5 m/s). These thermo-hygrometric conditions have been included in the measurements of the impulse responses in the bullring. As highlighted by Tronchin [47], in enclosures during the summer season, the sound strength and clarity parameters are less

dependent on changes in air velocity at low frequencies and more dependent at mid-high frequencies, while the opposite is stated for reverberation time parameters.

The bullring was acoustically excited to obtain the impulse responses (IRs) at the reception points by means of sine-swept signals of up to 30 s duration, wherein the frequency grows exponentially over time from 20 Hz to 20,000 Hz. These signals are provided and processed by the commercial software platform IRIS [48] for the 3D impulse responses connected to the rest of the measurement chain through MOTU 4PRE HYBRID. The excitation signal was reproduced in the space using an Omnipower 4292 dodecahedral sound source Type 4292-L, located 1.50 m above floor level, and amplified with a B&K 2734-type power amplifier. The 3D impulse responses were captured with the Core Sound TetraMic microphone array pointed in the same direction as the seat; this microphone allows temporal and spatial (3D) information to be incorporated. The intuitive and interactive visualization of 3D impulse response data in the form of an "intensity hedgehog" constitutes an interesting feature provided by the IRIS measurement software and shows the sound energy reaching the receiver position as a series of vectors or peaks, where the length of each vector indicates the level, the angle is the input direction, and the color corresponds to the arrival time. Through the inspection of these 3D hedgehogs, it is possible not only to visualize the link between architecture and sound spatiality and to observe the directional distribution of early and late energy but also, for example, to observe the extent of the lateral distribution of the initial reflections and the degree of diffusion of the sound field [49].

The IRIS system has the ability to ascertain the directional parameters (J_{LF} and L_J) directly. In the post-processing phase, IRIS automatically positions a virtual lateral figure-of-8 microphone. By analyzing the initial 2 ms of the recorded impulse response, the IRIS system identifies the direct sound and aligns the null position of the virtual lateral microphone in that specific direction. In order to measure parameters related to sound intensity (G), which involves comparing the energy of the impulse response measured within a room to the energy of the impulse response measured in a free field 10 m away from the sound source, a sound strength calibration is carried out in a semi-anechoic chamber.

In all cases, microphones were placed at 1.20 m from the floor except when placed in the passageway at 1.60 m.

Impulse responses recorded by the IRIS system show a sufficient range in the impulse-response-to-noise ratio (INR > 45 dB in each octave band) for the decay ranges in each band of interest. The background noise level was recorded with a PCE-430 Class I Sound Level Meter, averaging 5 min of background noise level and measuring 48.2 dBA.

3.4. Acoustic Simulation

For the simulation of the acoustic model, the commercial software ODEON Room Acoustics [44] version 17, based on GA, has been utilized. ODEON software employs algorithms that calculate early reflections by combining the Image Source Method (ISM) and the Early-Scattering Method (ESM), and by applying a stochastic scattering process using secondary sources. Late reflections are calculated via the Ray-Radiosity Method (RRM), where secondary sources radiate energy locally from surfaces and are assigned a directionality by considering scattering due to the size and surface roughness.

ODEON enables reliable predictions in rooms when the frequency band of interest is above four times the Schroeder frequency [23]. Since the lowest frequency (approx. 88 Hz) of the 125 Hz octave band is much higher than four times the Schroeder frequency of the bullring, approximately 11 Hz, considering the volume of the bullring as if it were enclosed, then the model provides reliable results above this octave band. In accordance with the recommendations of ISO 3382-1 [45], the frequency range involved in this study runs from 125 to 4000 Hz.

The source and receiver positions used in the acoustic simulation were the same as in the actual measurements, as illustrated in Figures 2 and 3. For each of the sources, two directivity patterns were defined: one radiating sound spherically "Omni", to obtain the acoustic parameters, with a gain of 31 dB, and another with a radiation diagram like that

of the human voice speaking aloud "BB93 Raised Natural", for the intelligibility values (STI), which provides a level of 66.5 dBA at a distance of 10 m. For this second purpose, the sources were also pointed at receiver R5 (as a representative position), and the noise registered during the measurements with a total SPL of 49.3 dBA was also established as background noise.

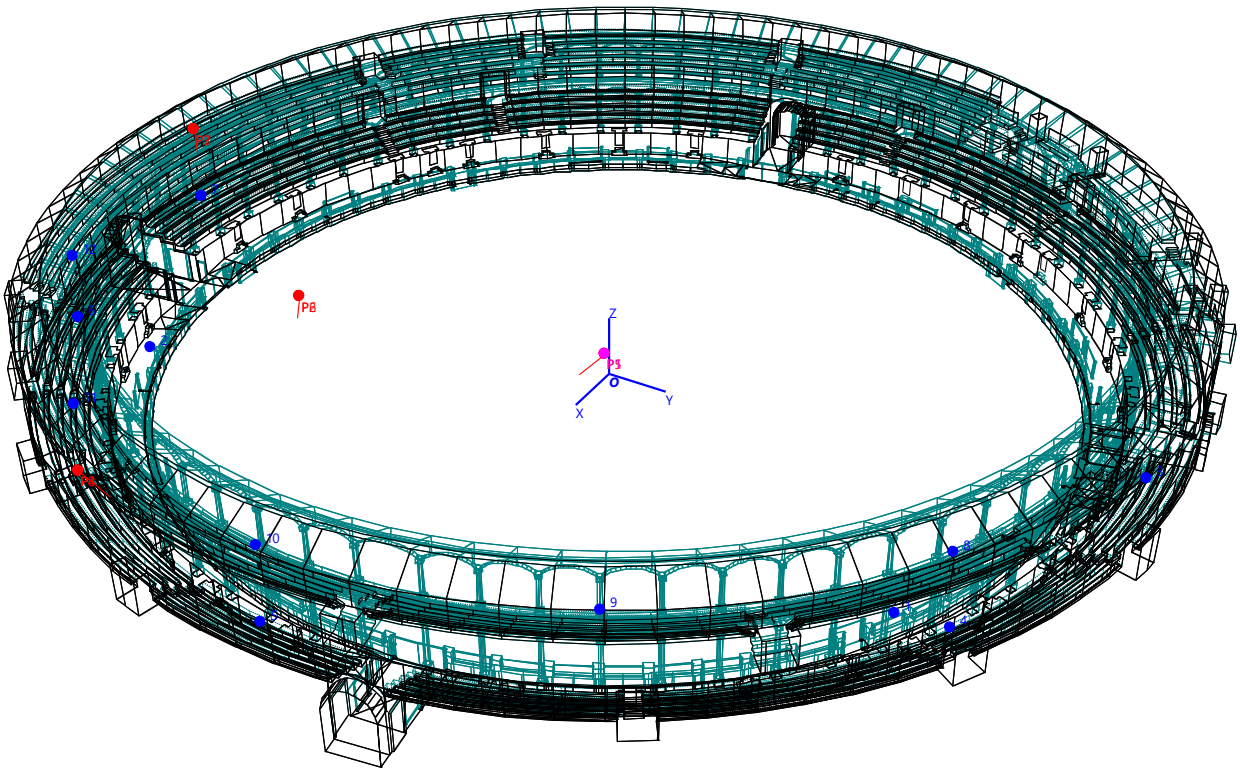

Figure 3. View of the acoustic simulation 3D model with the source (red) and receiver (blue) positions.

Most of the materials of the surfaces of the RMCR bullring have low absorption coefficients, except for the sand on the arena, the fictitious surfaces of the "ceiling" over the bullring, the holes in the vomitoria, and the public (if present). The absorption coefficients were obtained from the ODEON materials library, from the literature, as well as from previous experience in similar studies. Although the scattering coefficient varies with frequency, in ODEON, a single value corresponding to 707 Hz is assigned, which is distributed across the remaining frequencies. Hence, the lower frequencies have less scattering, while higher frequencies have higher scattering. In the simulation, the scattering coefficients suggested in the ODEON manual were used according to the roughness of the finishing surfaces. Scattering due to diffraction from effects such as distance, angle of incidence, and automatically calculated edge diffraction during ray tracing was also considered. Table 2 shows the random-incidence absorption coefficients (initial and optimized with calibration), the scattering coefficients, the relative percentages of surface area, and the corresponding reference.

ODEON defaults to all surfaces as normal type, which applies scattering and diffraction across the entire frequency range when the reflection-based scatter is enabled. By manually selecting the "open ceiling" surface as the Exterior type, less scattering is applied at low frequencies. The curved elements (columns and grandstand arches) were modeled as several small fractional surfaces to compensate for edge diffraction that these surfaces would cause individually. The smoothing of details in bases, capitals, and cornices was also compensated with a higher scattering coefficient.

Table 2. Relative surface percentages (%), scattering (s), absorption (α) coefficients, and wall types used in the simulations.

Materials		Area (%)	s	α						Type	Ref.
				125 Hz	250 Hz	500 Hz	1 kHz	2 kHz	4 kHz		
Sandstone (fractal)		1.9	0.01	0.02	0.02	0.03	0.04	0.05	0.05	fractional	[50]
Sandstone (bases capitals and cornices)		2.3	0.05	0.02	0.02	0.03	0.04	0.05	0.05	normal	[50]
Sandstone		2.6	0.01	0.02	0.02	0.03	0.04	0.05	0.05	normal	[50]
Granite stone		5.3	0.01	0.11	0.10	0.10	0.10	0.08	0.08	normal	[44]
Wood (barriers and gates)		2.6	0.01	0.14	0.10	0.06	0.08	0.10	0.10	normal	[23]
Concrete (screeds)		2.3	0.01	0.01	0.01	0.02	0.02	0.02	0.05	normal	[23]
Fir wood		4.3	0.01	0.10	0.10	0.10	0.09	0.10	0.12	normal	[50]
Vomitorium		0.6	0.01	0.80	0.80	0.80	0.80	0.80	0.80	normal	[51]
Ceramic (flooring)		6.2	0.01	0.02	0.02	0.02	0.02	0.02	0.02	normal	[50]
Ceramic (Arabic tile)		3.0	0.01	0.03	0.03	0.03	0.04	0.05	0.07	normal	[52]
Audience [1]		10.6	0.7	0.60	0.74	0.88	0.96	0.93	0.85	normal	[44]
Wood (floorboards)		0.6	0.01	0.10	0.07	0.05	0.06	0.06	0.06	normal	[44]
Mortar render		13.0	0.01	0.12	0.10	0.08	0.06	0.06	0.06	normal	[50]
Gypsum plaster		4.6	0.01	0.02	0.02	0.03	0.04	0.05	0.05	normal	[23]
Albero (sand soil) [2]	Init.	14.8	0.01	0.02	0.21	0.23	0.23	0.20	0.08	normal	[53]
	Opt.			0.02	0.22	0.27	0.25	0.23	0.10		
Open ceiling [2]	Init.	19.9	0.01	1.00	1.00	1.00	1.00	1.00	1.00	exterior	-
	Opt.			0.86	0.90	0.95	0.93	0.93	0.92		
Gypsum plaster + wood [3]		5.1	0.2	0.07	0.06	0.04	0.06	0.07	0.07	normal	-

[1] In simulations without an audience, the chosen material is "transparent" with absorption coefficients equal to 0 at all frequencies. [2] Material coefficients used for the adjustment of the model. [3] Obtained by a combination of gypsum plaster (53.9%) and wood lattice (46.1%).

In order to obtain the most accurate results possible, the Simulation Parameter Investigation tool from ODEON was employed to investigate how the number of rays and the order of transition occurred in agreement between the simulations and the in-situ measurements. The tool displays different curves for different transition orders, thereby helping to determine the optimal number of rays and transition order for the simulations. In this way, the transition order was set to 2, and 1 was discarded since it reduced the representation of the first reflections by the image source method. The number of late rays was increased to 1,150,000 to ensure that the reflection density parameter remained greater than 100 reflections/ms and that the decay curves presented no bumps or abrupt drops. The duration of the impulse response was fixed at 2400 ms. Background noise temperature and relative humidity were set to the average thermo-hygrometric conditions, measured in situ.

4. Experimental Results and Discussion

The acoustic study of performance spaces is frequently carried out on the basis of a set of parameters obtained from the measurement of impulse responses, which in turn are related to subjective aspects of their aural architecture. These acoustic descriptors defined in ISO 3382-1 [45] generally include acoustic parameters or descriptors based on decay time, EDT, T_{20}, and T_{30}; energy parameters, G, C_{80}, D_{50}, and T_S; and directional parameters, J_{LF} and $L_{J,}$ among others. Furthermore, the speech transmission index, STI, is used as the speech intelligibility parameter in accordance with the IEC 60268-16:2020 standard [54].

The ISO 3382-1 standard mainly applies to enclosed spaces, where there is a widespread consensus on its validity for the assessment of their acoustic behavior. However, there are currently uncertainties when evaluating the acoustics of unroofed spaces using the parameters defined in said standard since these spaces have a significantly different characteristic sound field compared to the reverberant field of enclosed spaces. While the averaged reverberation time works well as a global descriptor of the acoustics in enclosed rooms due to its small spatial variations, other parameters, such as EDT, subjectively related to perceived reverberance, clarity, or sound intensity, have recently been questioned as to their suitability as parameters for the evaluation of the acoustics of open-ceiling spaces [55].

With few exceptions, acoustic descriptors are traditionally calculated by integrating the sound energy of impulse responses over time; this makes them unsuitable for investigating acoustics in detail, especially in the early part of the impulse response [19], where early reflections define the acoustic signature of any room.

The complete description of the spatial propagation of sound is obtained from the 3D impulse response by placing sources and receivers in several relevant positions and analyzing the distribution of sound energy in the time-frequency and spatiotemporal domains, thereby overcoming the lack of detail of the standard analysis.

4.1. Main Measured Acoustic Descriptors

Table 3 presents the impulse-response-to-noise ratio, INR of the recorded impulse responses, and several acoustic descriptors considered in the present study related to reverberation, EDT, and T_{30}, and to sound clarity, evaluated through the parameters C_{80} and D_{50}. The plotted graph of parameter C_{80} highlights the measurements obtained with the source at position S3, where the music band is located. Certain analyses related to the perceived spatial sensation are also carried out, using the apparent source width of the source, J_{LF} descriptor, and the listener's envelope, L_J. In all cases, the spatial dispersion is studied through the standard deviation and the perceptual differences in terms of the ratio between the standard deviation and the corresponding JND of the parameter expressed in ISO 3382-1. Values are presented in octave frequency bands between 125 and 4000 Hz and as a single-number frequency average, along with the standard deviation (in parentheses). These ratios are presented for a total of 48 source-receiver combinations for decay time parameters and 39 source-receiver combinations for the remaining parameters.

Table 3. Overall results of measurement. Values in frequency octave bands averaging for all sources and receivers, standard deviation (in parentheses), number of JNDs of this deviation, and single-number frequency averaging in accordance with ISO 3382-1 [45].

		Frequency						**Single Number**
		125 Hz	**250 Hz**	**500 Hz**	**1 kHz**	**2 kHz**	**4 kHz**	
INR	[dB]	55.8 (5.7)	60.6 (4.8)	60.4 (5.2)	59.3 (5.6)	65.0 (5.4)	64.9 (4.4)	-
T_{30}	[s]	2.66 (0.20)	2.24 (0.18)	1.99 (0.14)	1.96 (0.13)	1.83 (0.12)	1.66 (0.12)	1.98 (0.14)
	N°. JND	1.5	1.6	1.4	1.3	1.3	1.4	1.4
EDT	[s]	2.46 (1.46)	1.94 (0.99)	1.73 (0.78)	1.73 (0.76)	1.57 (0.77)	1.35 (0.65)	1.73 (0.77)
	N°. JND	11.9	10.2	9.0	8.8	9.8	9.7	8.9
C_{80}	[dB]	2.2 (6.5)	2.9 (5.1)	2.6 (2.9)	4.4 (3.0)	5.1 (3.9)	4.7 (3.4)	3.5 (3.0)
	N°. JND	6.5	5.1	2.9	3.0	3.9	3.5	3.0
D_{50}	[-]	0.50 (0.22)	0.52 (0.19)	0.54 (0.17)	0.57 (0.16)	0.62 (0.16)	0.62 (0.17)	0.56 (0.17)
	N°. JND	4.4	3.8	3.4	3.3	3.2	3.4	3.4
J_{LF}	[-]	0.18 (0.14)	0.16 (0.11)	0.17 (0.10)	0.17 (0.09)	0.19 (0.11)	0.21 (0.11)	0.17 (0.11)
	N°. JND	2.8	2.2	1.9	1.8	2.3	2.2	2.2
L_J	[dB]	−1.5 (3.0)	−7.5 (3.3)	−10.8 (3.2)	−11.7 (2.7)	−9.0 (2.6)	−4.4 (3.0)	−5.9 (3.1)
	N°. JND	3.0	3.3	3.2	2.7	2.6	3.0	3.1

These previous results are expanded and refined by means of graphs where the average values for each of the sound sources have been plotted. In this case, there are four source positions (for the energy parameters, average values of 11 measurements for S1, 11 measurements for S2, eight measurements for S3, and nine measurements for S4), and hence four curves are plotted. In all the plotted graphs of the acoustic parameters, the horizontal marks correspond to the standard deviation values (Figure 4).

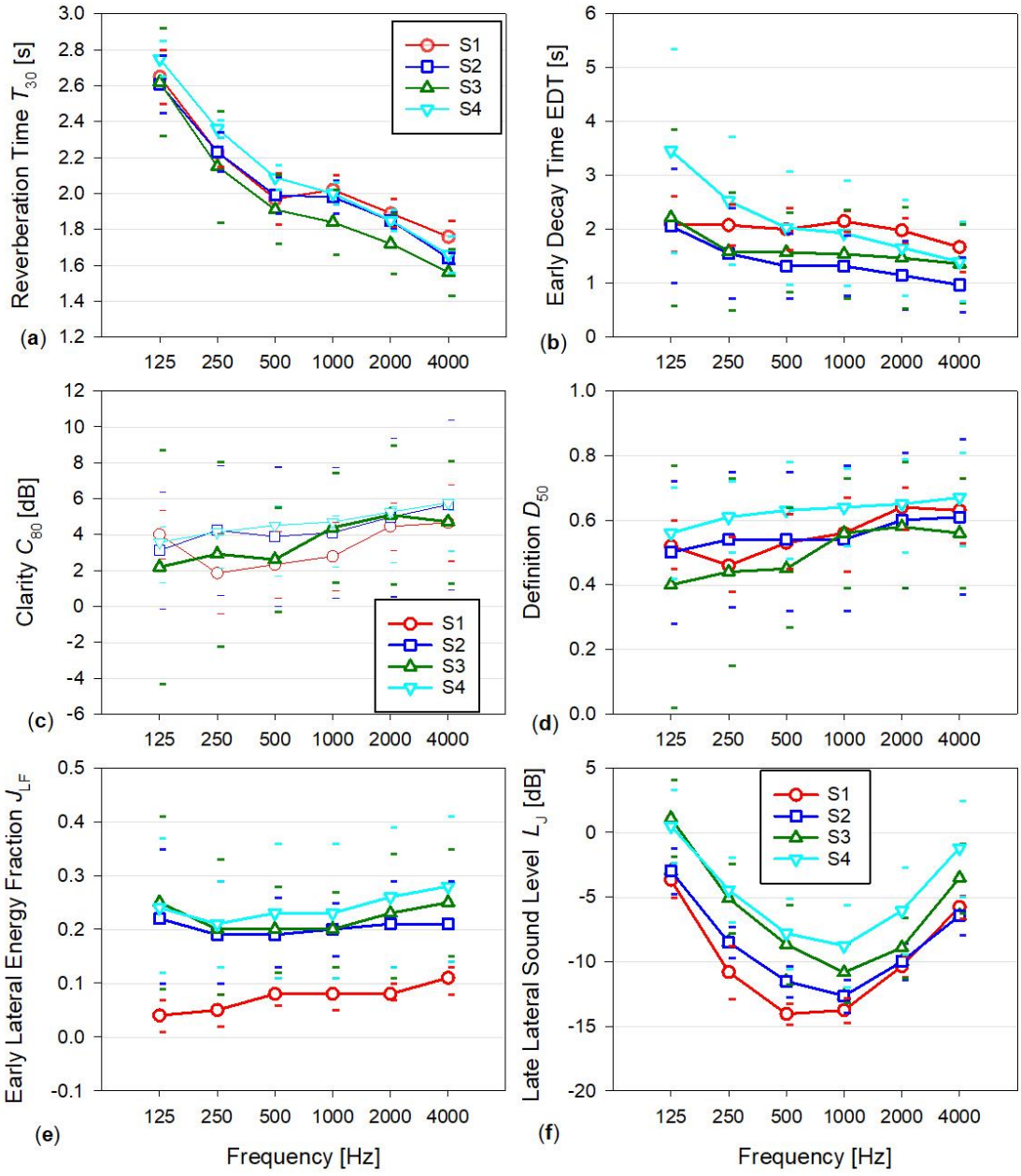

Figure 4. Spatial averages of the measured acoustic parameters as a function of frequency for the four sources S1–S4: (**a**) Reverberation Time; (**b**) Early Decay Time; (**c**) Clarity, highlighting S3 results; (**d**) Definition; (**e**) Early Lateral Energy Fraction; (**f**) Late Lateral Sound Level.

The linearity of the energy decay curves is evaluated by using the degree of curvature C and the degree of non-linearity ξ for the parameter T_{30}, defined in Annex B of ISO 3382-2 [46]. Of these linearity values, 74.7% (48 source-receiver combinations and six-octave bands) meet the linearity criteria of 0–5% and 0–5‰, respectively, for both parameters. The linearity threshold, established at 10% for C and 10‰ for ξ, is exceeded by 8.7% of the values, which casts doubts on the T_{30} results corresponding to these decay curves. The high degree of linearity in the time-energy decay curves is due to the fact that most of the audience is seated inside the galleries, and hence, the late energy has sufficient input compared to that which occurs in open spaces, such as Greek and Roman theaters. The most outstanding non-linearity occurs in the extreme bands of 125 and 4000 Hz. There are two combinations, S2–R12 and S3–R12, where the degree of non-linearity ξ exceeds the

threshold of 10‰ for the six-octave bands, possibly due to poor visibility and proximity between source and receiver, respectively.

Figure 4a,b show the spatially averaged T_{30} and EDT of measured results for each sound source. In open bullrings, the reverberation time depends little on the location of receptors, as shown by the similarity of the different curves obtained and low spatial dispersion. However, the values of T_{30} corresponding to the S3 source, where the music band is located, are slightly lower. The average reverberation time T_{30m} is 1.98 s (spatial average of the 48 source-receiver combinations, at frequencies of 500 and 1000 Hz), with similar spatial dispersion at all frequencies. In contrast, the EDT parameter, related to the listeners' perceived reverberation, proves to be more dependent on location. Similarly, the mean early decay time $\mathrm{EDT_m}$ is 1.73 s, with much greater spatial dispersion at all frequencies, especially at low frequencies. The significant variability observed indicates that EDT provides a warning that these global average values for the entire space must be used with extreme care [54].

The spatially averaged C_{80} and D_{50} results for each sound source and octave band are shown in Figure 4c,d. For parameter C_{80}, which is subjectively associated with perceived musical clarity, and where clarity and reverberation are opposite perceptual attributes, the higher the reverberation, the lower the clarity (and vice versa), and therefore a simultaneous meeting point is desirable in this type of space. The graph of parameter C_{80} highlights the curve corresponding to position S3, where the music band is located. The mean clarity, C_{80m} of the bullring is 3.5 dB (frequency average of a single number), and the spatial dispersion corresponding to the mean value of source S1 is 3.0 JND, while the other sources S2, S3, and S4 present dispersions of 3.8, 3.0, and 2.7 JND, respectively. One key aspect of this parameter is that in open-ceiling spaces, the late energy can be extremely low or non-existent, resulting in C_{80} values that can reach high dB levels (approaching infinity), which is clearly not significant. However, in this space, due to the receptors being immersed in the gallery, there is a sustained level of sufficient late energy, as is evident from the linear decay observed. Regarding D_{50}, speech definition, the spectral behavior is very similar to that of C_{80}. The average value of D_{50m} for the entire bullring is 0.56, and the spatial dispersion of the whole is 3.4 JND. This presents a behavior for the sources similar to clarity, with 2.0 JND for S1 and dispersions of 4.5, 3.6, and 2.7 for S2, S3, and S4, respectively. This indicates that D_{50} is a meaningful descriptor for the characterization of speech definition in this particular space [55].

The spatially averaged results for each sound source of the directional parameters related to the subjective aspects of apparent source width, J_{LF}, and the listener envelope, L_J, are shown in Figure 4e,f, respectively. Once again, the most unfavorable values are presented for position S1 due to the reduced lateral sound effects in comparison to other configurations, which gives the subjective impression that the sound source is less wide or is smaller in the center of the ring, in keeping with the spectacle, where the sound sources correspond to the bull and the bullfighters. For the bullring, the single-number value of the early lateral energy fraction, J_{LFm}, is 0.17 (arithmetic average for the four-octave bands from 125 to 1000 Hz), with smaller spatial dispersion for source S1 than for sources S2, S3, and S4. The impression of being surrounded by the sound field, evaluated by the parameter L_J, late lateral sound level, presents differences ranging between +1.1 and −14.5 dB for the values averaged per source, with maximum levels at extreme frequencies and minimum levels at mid frequencies. The value of L_J expressed as a single number is −5.9 dB (energy average for the four-octave bands from 125 to 1000 Hz).

According to the last column of Table 3, the single-number parameters in this bullring present values for each parameter that lie within the typical range indicated in ISO 3382-1 for non-occupied concert and multi-purpose halls of up to 25,000 m^3: T_{30m} 1.98 s, Gade [56] recommends 2–2.4 s for a ratio of 25,000 m^3/2000 seats for symphony music, (compared to Roman theaters, whereby Carthago Nova theater has 1.86 s and Saguntum theater has 2.23 s, both in Spain [49], while Aspendus theater in Turkey [57] has 1.70 s); $\mathrm{EDT_m}$ 1.73 s, typical range 1–3 s; C_{80m} 3.5 dB, typical range −5 dB to +5 dB (compared to Roman theaters,

whereby Carthago Nova theater has 8.9 dB and Saguntum theater 1.33 dB, both of which are in Spain [49]); D_{50m} 0.56, typical range 0.3–0.7 (compared to Roman theaters whereby Carthago Nova theater has 0.80, Saguntum theater 0.49, both of which are in Spain [49], while Aspendus theater in Turkey [57] has 0.70); J_{LFm} 0.17, typical range 0.05–0.35 and within the range recommended by Gade; L_J energy average −5.9 dB, typical range −14 dB to +1 dB; G_{mid} −0.34 dB, whose typical range is −2 dB to +10 dB.

Lastly, various analyses were carried out based on source-receiver distance, the speech transmission index STI, and the sound strength G_m (average frequency of 500 and 1000 Hz); see Figure 5a,b. The STI is calculated from the impulse response measured with the IRIS system following the indirect method validated by Cabrera et al. [58]. The STI has been estimated for a given voice level (Loud Speech Effort), and background noise has been measured in situ. The majority of the results lie within the good-fair range despite the long distances. Regarding the subjective level of sound of this space, evaluated through the sound strength G_m, the measured values for the 39 source-receiver combinations are represented, differentiated for each of the four sources together with the theoretical propagation of sound in free field and in the classic diffuse field model of closed rooms. For this calculation:

$$G(\mathrm{r}) = 10 \log (100/\mathrm{r}^2 + 31{,}200T/V)\ (\mathrm{dB}), \quad (1)$$

a volume of the bullring of V = 69,237 m^3 and T_{30mid} averaged for each source have been considered. The values of T_{30mid} are nearly the same for all four sources, and hence, so are the curves. Most of the experimental results show a level below the diffuse field result, while several results for certain sources, especially S3, are above this level.

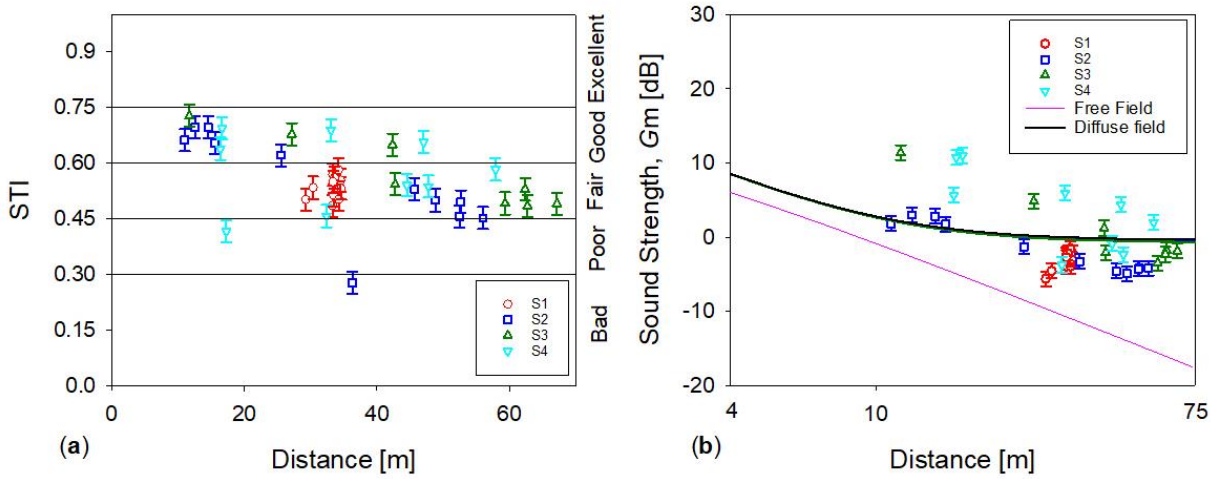

Figure 5. Measured acoustic parameters as a function of source-receiver distance for the four sources S1–S4: (**a**) Speech transmission index; (**b**) Mean-sound strength; solid lines show other theoretical behaviors. Error bars correspond to their JNDs.

The results of G_m versus distance show the variations depending on the proximity to the source and the contribution of the energy reflected in the space where the floor of the arena and the interior façade with galleries at two heights predominate.

4.2. Acoustic Signature

The *acoustic signature* of the RMCR bullring, obtained from the information provided by the early reflections from the 3D impulse response, was performed by analyzing the distribution of sound energy in the time-frequency and space-time domains [19,21]. The levels and relative delays of the reflections that arrive after direct sound have been studied through the frequency response (RFR) derived from the room impulse response (RIR). All receiving positions present behavior of their analogous RFRs, with a very similar pattern of the frequency spectrum. As an example, Figure 6 shows the RFR magnitude curves within

time windows corresponding to receiver R5 for the four sound sources, S1 to S4. Each curve indicates the responses within a time window from the initial direct sound to 20, 50, 80, 200 ms, and to the final time.

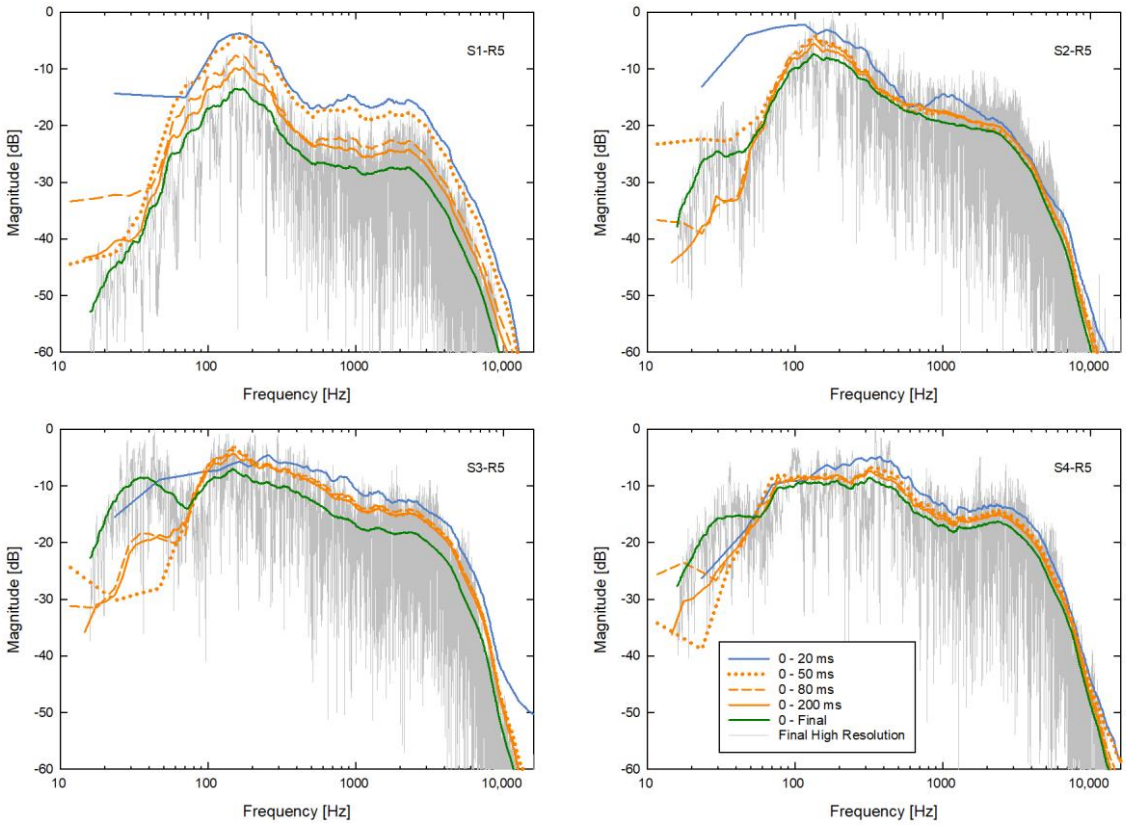

Figure 6. Frequency responses corresponding to receiver R5 for the four sound sources, S1 to S4, smoothed in 1/1 octave bands.

The selection of 20 ms as the duration of the first-time window is due to the precedence effect in the human ear that merges the first reflections with the direct sound. The 50 and 80 ms curves are associated with the early energy limits of speech and music clarity, respectively. The upper limit of 200 ms is associated with the initial margin of −5 dB in the commonly used linear fit for reverberation-time estimates. Finally, the cumulative frequency response curve after 200 ms represents the energy of the diffuse or late reverberant sound.

In the four graphs of the measurements obtained in the R5 receiver, the RFR curves are characterized by an appreciable drop between 200 and 1100 Hz caused by sound diffraction from the rows of seats of the early reflection sound coming from the arena, similar to those studied in classical theatres [59–61]. The overlap of direct and delayed sounds causes destructive interference, resulting in substantial level attenuation that varies significantly in frequency when switching from one source to another.

Although this characteristic affects the level of voice and the frequency content of vowels of the human voice, nevertheless, according to the spectra, the different orders of reflections and edge diffraction in the grandstands enhance spectral content in the high-frequency region, which is vital for the intelligibility of speech as indicated by the acceptable and good values of the STI parameter even at great distances from the source.

The frequency-domain analysis above is corroborated by the spatiotemporal simplified description performed in this study. The IRIS [48] three-dimensional impulse-response measurement system can determine the direction of incoming sound at the measurement position using a sound intensity technique. The display of sound arriving at the receiver is represented as a series of linear vectors known as "intensity urchins" on a 2D or 3D

Cartesian diagram. The length of each vector indicates the magnitude, the angle is the direction, and the color corresponds to the time of arrival. In the measurements studied, a 2 ms time window was used, which restricts the analysis to frequencies of 500 Hz and above, and the vectors were colored according to the following time intervals: 0–2 ms, Red; 2–15 ms, Green; 15–50 ms, Dark Blue; >50 ms, Blue (Figure 7b).

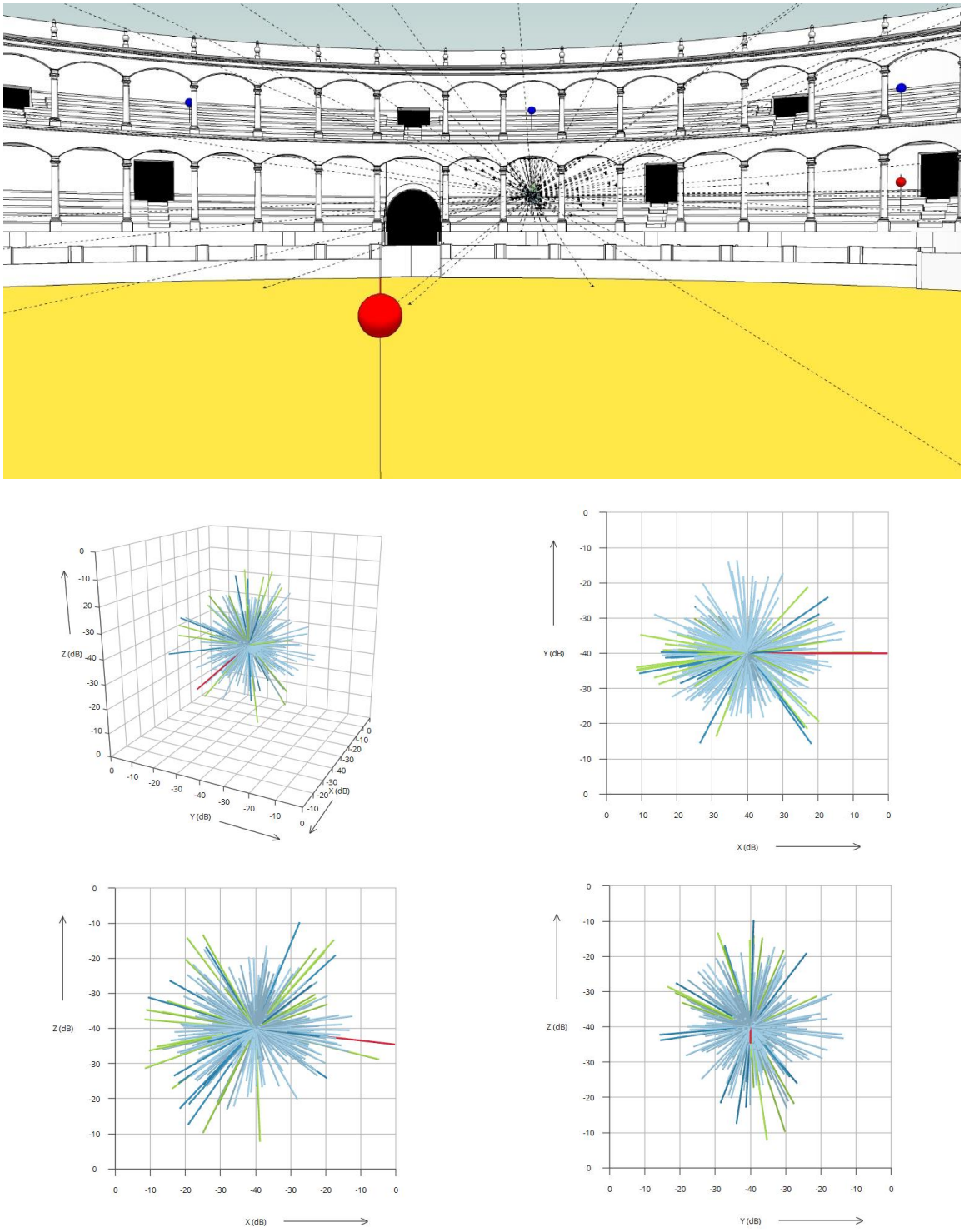

Figure 7. Diagram of broadband extended intensity lines in the geometric model for the S1–R5 combination: (**a**) view from the center of the arena; (**b**) From left to right and top to bottom, the 3D, XY, XZ, and YZ Cartesian diagrams of IRIS, the "speech" time window used in the analysis.

It is worth bearing in mind that a single line represents the average sound intensity over the respective 2 ms time window. Each line must not be taken as representing an individual reflection since, in many cases, a time window may include more than one reflection, and the resulting line will indicate the average level and direction of all included reflections. The "intensity hedgehogs" were primarily utilized to identify significant reflections and the cause of the reflections related to the architecture of the bullring, and secondly to determine where early and late energy comes from and how this distribution changes over time.

All broadband "intensity hedgehogs" are exported to Sketchup modeling software to visualize the link to the architecture. The time intervals are organized in layers, which can be shown and hidden for ease of analysis, and the intensity lines extend to the limits of the geometric model, appearing as a cross at the intersection with the surface. As an example, Figure 7 shows the "intensity hedgehog" of the S1–R5 combination for the "speech" time window, together with the 2D and 3D IRIS Cartesian diagrams. For the sake of simplicity, late reflections have been omitted.

The spatial and temporal energy analysis for the S1–R5 combination confirms the result of its frequency response by graphically showing how the acoustic reflections are distributed on the rows of seats and the back wall, responsible for the overlap and interference with the sound that comes from the source. This effect is noticeably improved when the sources move from the center of the arena. In most receivers, early energy has a front and rear spatial origin. Late energy, with less energy input, provides the lateral energy. It can also be observed in receivers R1 and R2 (passageway) that practically no reflections come from the upper part, as would correspond to an open space without a roof.

5. Results from the Acoustic Simulations and Discussion

5.1. Calibration

The calibration of the acoustic model was carried out by evaluating the similarity between the measured and simulated values of reverberation time (T_{30}) and musical clarity (C_{80}), which usually show a strong negative correlation with each other: the higher the reverberation, the lower the clarity (and vice versa), in order to achieve a meeting point between these two perceptual attributes in a consistent way. The four sound sources and all the source-receiver combinations with direct sound in Table 1 were taken into account. Calibration was considered achieved when most of the differences between the measured and simulated values, for each octave band between 125 and 4000 Hz, and for all source-receiver combinations, came within twice the JND [23]. In this case, 10% for T_{30} and 2 dB for C_{80}. Although this study has taken into account the perceptual thresholds of ISO 3382-1, recent research with different stimuli, listening tests, and evaluator quantities suggests the existence of larger increases in JND than that which has been previously reported in the literature [62–64]. These differences enable the estimation of the uncertainty of not only the measurements taken in situ to be considered but also that of the sources of uncertainty inherent in commercial software [33,34].

The process consists of quantifying the sensitivity of the acoustic model to variations in the absorption coefficients of those materials that generate the most uncertainty through the execution of simulations and successive adjustments within reliable ranges until the calibration is achieved. The optimized simulation was reached from the initial simulation of 24.36% differences for T_{30} and 57.26% differences for C_{80} to 81.62% and 58.55%, respectively, for a total of 234 differences (39 source-receiver combinations and six-octave bands), see Table 4.

The results are also analyzed separately for each source S1, S2, S3, and S4, and the coincidence is highlighted between simulated and measured values of the combinations corresponding to S4 (98.15% for T_{30} and 72.22% for C_{80}), followed by the sources S1 and S2. Figure 8 shows the comparison between the measured and simulated average values of reverberation time (T_{30}) and musical quality (C_{80}) for each source position. It can be observed that, with the adjustment made, a high degree of concordance between the

measurement and the simulation for all the source-receiver combinations has been achieved. The remaining acoustic descriptors follow the same trend, whereby most of the differences are left within twice their corresponding JND (Early Decay Time, EDT: 37.44%; Center Time, T_S: 57.89%; Sound Strength, G: 30.53%; Definition, D_{50}: 63.15%; and Clarity for speech, C_{50}: 62.02%).

Table 4. Measured and simulated results and JND in octave bands and as a single number for the evaluated acoustic parameters, corresponding to the Initial and Optimized simulations. Percentage of differences that verify the calibration criteria via sources S1 to S4 and global value. (The results of <2 JND are given in bold).

		Frequency [Hz]						Single Number	% Diff < 2 JND				
		125	250	500	1000	2000	4000		S1	S2	S3	S4	Global
T_{30} [JND = 5%]	Meas. [s]	2.66	2.24	1.99	1.96	1.83	1.66	1.98					
	Sim. Init. [s]	1.90	1.83	1.80	1.75	1.66	1.46	1.78					
	Diff. Init. (JND)	5.70	3.62	**1.89**	2.20	**1.91**	2.42	2.04	10.61%	25.76%	41.67%	24.07%	24.36%
	Sim. Opt. [s]	2.59	2.26	2.10	2.05	1.92	1.67	2.08					
	Diff. Opt. (JND)	**0.52**	**0.26**	**1.11**	**0.86**	**0.96**	**0.17**	**0.99**	83.33%	87.88%	52.08%	98.15%	81.62%
C_{80} [JND = 1 dB]	Meas. [dB]	3.3	3.3	3.3	3.9	4.9	5.2	3.6					
	Sim. Init. [dB]	3.8	3.9	3.9	4.1	4.5	5.4	4.0					
	Diff. Init. (JND)	**0.49**	**0.60**	**0.59**	**0.15**	**0.40**	**0.21**	**0.37**	51.52%	60.61%	54.17%	62.96%	57.26%
	Sim. Opt. [dB]	2.0	2.7	3.1	3.3	3.8	4.7	3.2					
	Diff. Opt. (JND)	**1.32**	**0.55**	**0.17**	**0.63**	**1.12**	**0.49**	**0.40**	43.94%	65.15%	54.17%	72.22%	58.55%

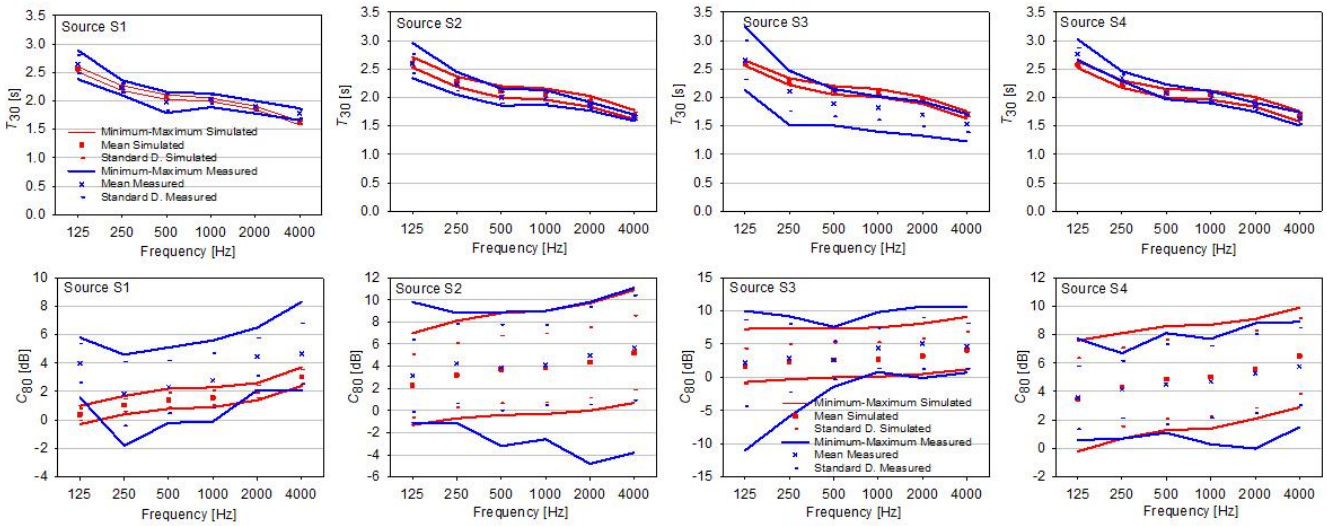

Figure 8. Comparison between spatially averaged measured and simulated values obtained for the reverberation time (**upper row**) and the clarity (**lower row**) and for each sound source S1, S2, S3, and S4.

5.2. Simulations with the Various States of Occupancy

In order to complete the sound characterization of the Ronda bullring, the results of the acoustic simulations are presented and discussed, and the influence of audience occupancy and vacancy are compared, as are the variations due to the location of the various sound sources that exist in the performance of the on-foot bullfighting.

The results of the simulations are presented using the color maps provided by the ODEON program. The most relevant horizontal surfaces have been selected as those defined by the audience areas of the lower and upper grandstands, the passageway, and, additionally, to facilitate analysis, the arena. The height at which the grid floats has been set at 1.2 m for seated people and 1.6 m for standing people. Grid density has been adjusted to 1 m between receivers, which enables a trade-off between a fine-mesh grid and undue

computation time and results in a smooth interpolated grid without an excessive number of elements.

Table A1 in the Appendix A presents the average values obtained from the color maps for the two states of occupancy and for the four source positions of the main acoustic descriptors. The values are presented in frequency octave bands between 125 and 4000 Hz for a total of 3659 receivers. The average values of the STI obtained for a given voice level (Loud Speech Effort) and the background noise measured in situ are also included.

The grid responses of the interpolated results of the parameters T_{30}, D_{50}, C_{80}, and STI are displayed using color scales for the occupied and unoccupied states of the audience and for the four source positions S1, S2, S3, and S4. However, it should be noted that the parameter C_{80} is only presented for source position S3, where the music band is located. The default color scale and manual color scale ranges have been used for ease of comparison. Furthermore, their rating scale was used for STI, whereby each color represents a descriptive quality of speech intelligibility.

As expected, the presence of the public modifies the results of all the parameters and, therefore, improves the associated attributes of the sound sensation. The results obtained related to reverberation, EDT, and T_{30} show only small variations between octave bands but reveal significant differences depending on the audience area. Thus, for the simulation without occupancy, the average values of T_{30} oscillate between 2.6 s for 250 Hz and 1.6 s for 4000 Hz in the simulation without occupation, while with an audience, these are between 1.9 s and 1.3 s, respectively. Figure 9 shows the distribution in terms of zones of T_{30} (average), where it can also be appreciated that, for sound source S1, values lower than 1.3 are located. This is in contrast with the results for the EDT parameter in the closest locations to the source (arena), whereby the values are greater than 1.5 s in the areas furthest from the source, passageway, and grandstands. The increase in EDT results with the presence of the audience (added absorption), which only occurs when the sound source is in the center of the arena and never occurs in any of the other configurations. This anomaly is due to the simulation since no real measurements were made for the areas close to S1, which causes the averages that appear in Table A1 to be so high. The significant variability observed indicates that EDT must be used with extreme caution [55].

The clarity of sound, evaluated through parameters C_{80} and D_{50}, presents results in accordance with the greater or lesser absorption provided by the audience according to their state of occupancy and with the location of the source. The average values of C_{80} of the simulation without occupation are between 1.2 dB for 250 Hz and 3.9 dB for 4000 Hz, while in the simulation with occupation, this figure oscillates between 3.8 dB and 6.7 dB at identical frequencies. For D_{50}, analogously, the average values oscillate between 0.4 and 0.5 and between 0.6 and 0.7 for the simulation without and with occupancy, respectively. Figure 10 shows the color map of definition D_{50} for source positions S1, S2, and S4, and clarity C_{80} (average) (dB) for source position S3, with occupied and unoccupied audience area, and where especially for S3 and S4, the acoustic visibility zones and the shadow zones produced by the columns of the archway can be appreciated.

In order to conclude this discussion, the results of speech intelligibility with a human directivity source are analyzed using the STI index under the simulation conditions described in Section 3.4. The average value of STI for the simulation without occupancy is between 0.52 and 0.58, while in the simulation with occupancy, this lies between 0.61 and 0.64. The color maps of STI for the two states of occupancy and for the four sound sources are shown in Figure 11, together with the scale where each color represents a descriptive quality of speech intelligibility. It can be observed that the intelligibility decreases from the closest zones to the source, reaching values of the STI index qualified as excellent (dark green), going through the intermediate zones, qualified as good (light green) and fair (yellow), up to the most remote areas classified as poor (orange). It should be noted that no simulation has classified grids as having bad intelligibility (red). The influence of the state of occupancy is also observed, whereby larger areas with better intelligibility of speech are obtained with occupancy than those areas without an audience. In the simulations with

sources S3 and S4, the zones of acoustic visibility and shadow produced by the diffraction caused by the columns of the arcade can also be appreciated.

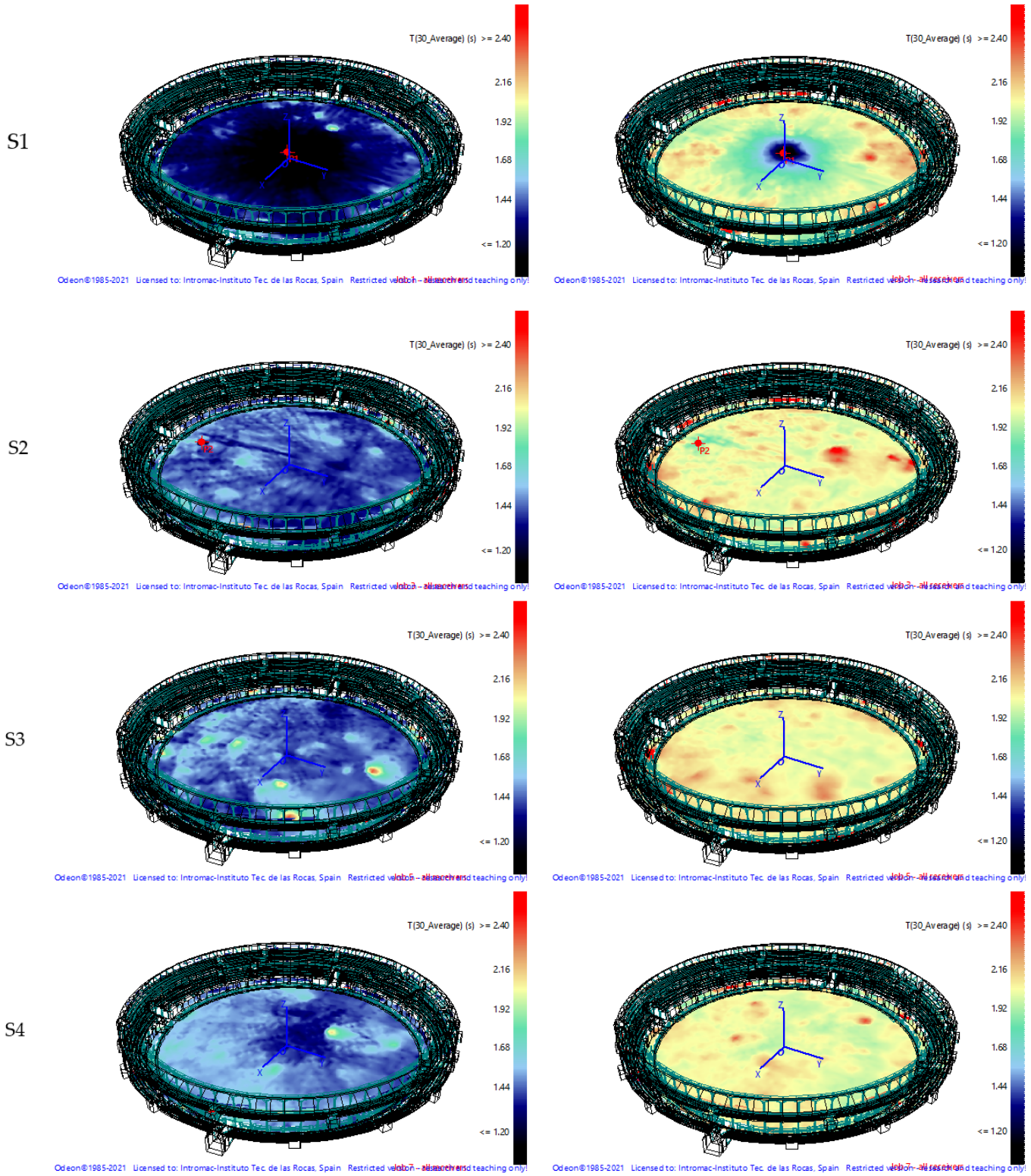

Figure 9. Grid responses for the reverberation T_{30} (average) (s) with occupied (**left-hand side**) and unoccupied (**right-hand side**) audience area and for the source positions S1, S2, S3, and S4.

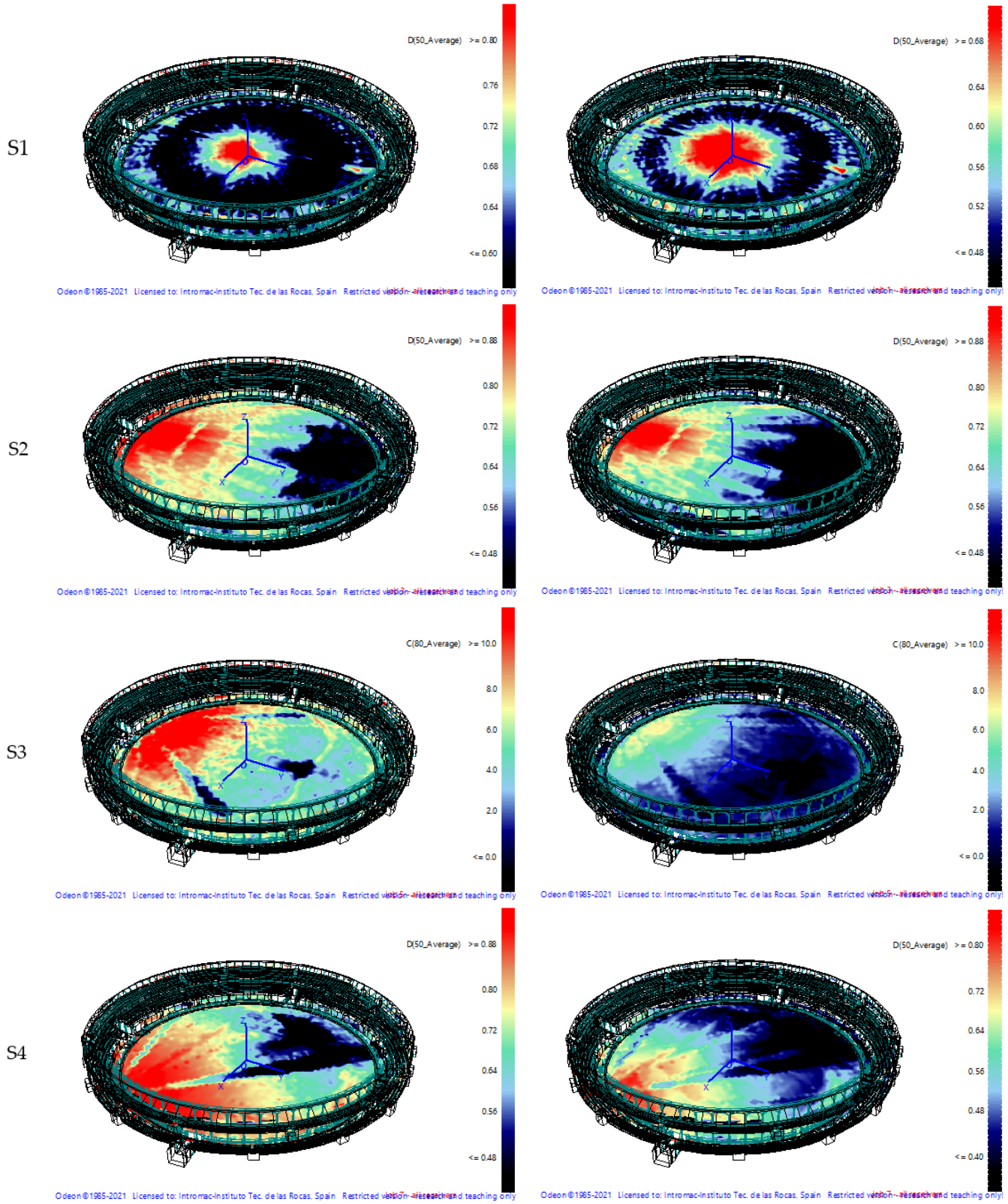

Figure 10. Grid response for definition D_{50} for the source positions S1, S2, and S4, and clarity C_{80} (average) (dB) for the source position S3, with occupied (**left-hand side**) and unoccupied (**right-hand side**) audience area.

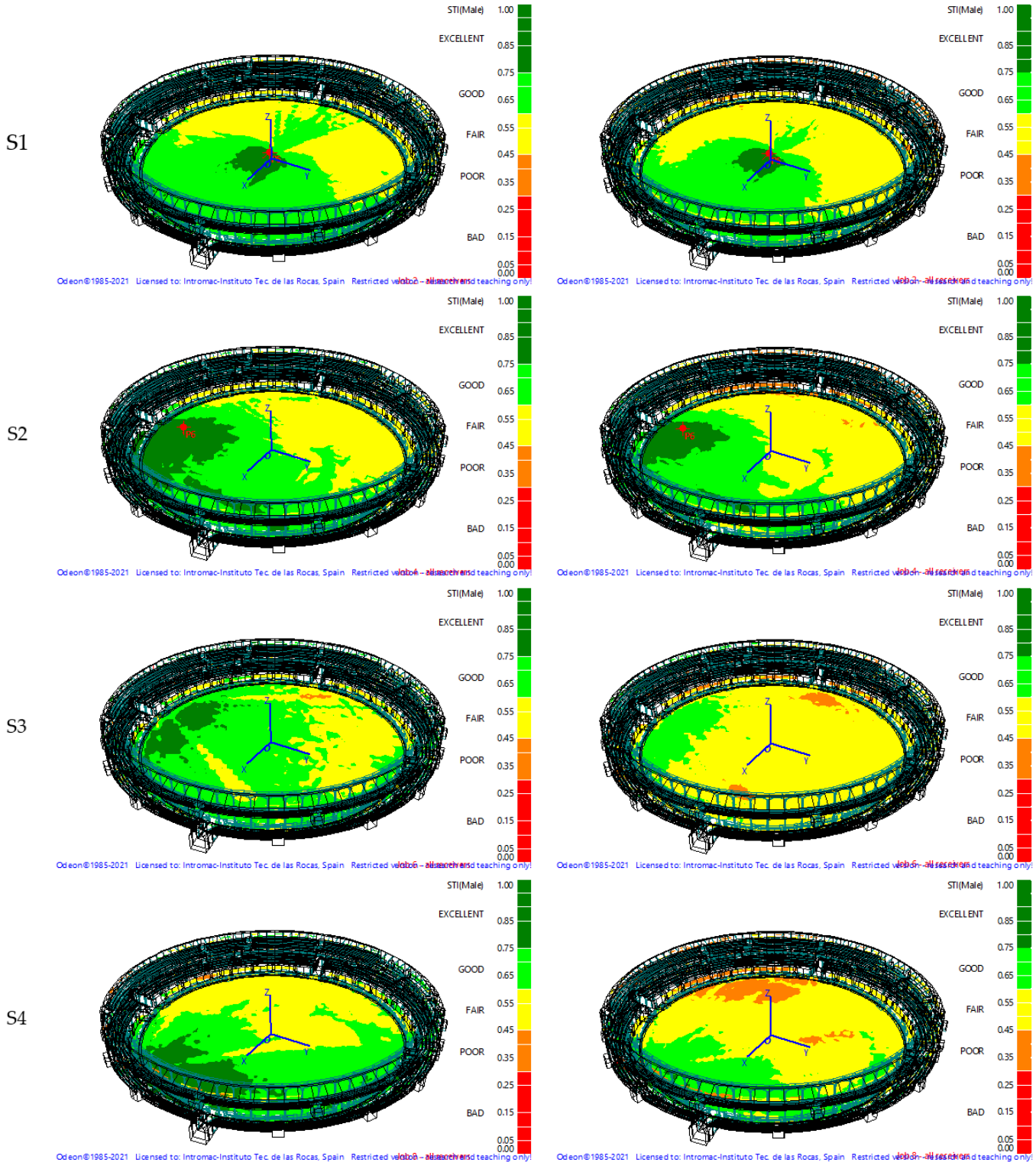

Figure 11. Grid response for the STI parameter of intelligibility with occupied (**left-hand side**) and unoccupied (**right-hand side**) audience area and for the source positions S1, S2, S3, and S4.

6. Conclusions

In this article, the acoustics of the bullring of Ronda have been studied: a monument declared an Asset of Cultural Interest, which stands out for its history, its architecture, and its beauty. The singularity of the sound architecture of this space has been analyzed from the parametric acoustic description and the spatiotemporal and spectrotemporal

analysis of the 3D impulsive responses measured in the absence of the public. The acoustic characterization is completed with the simulations of the digital model and validated with the experimental measurements, whereby the presence of the public and the different sound sources that exist in the development of the bullfight are analyzed, thereby contributing to the safeguarding of its acoustic heritage. As indicated in Section 1, Gerzon [12] promotes the preservation of acoustic heritage through the systematic collection of 3D impulse response measurements in order to assess the behavior of unique buildings and preserve them for posterity. In this regard, up to 48 3D impulse responses have been measured in this work for archival and preservation purposes.

The study has concluded that the acoustics of these unique performance spaces, although they do indeed share similar considerations to other outdoor venues designed for listening, such as ancient theatres and amphitheaters, possess a significant difference with said theaters since they host almost all members of the audience in their galleries. This fact makes it possible to maintain a greater contribution of late energy over time. This manuscript adopts the methodology for the acoustic characterization of bullrings that the authors have been developing in this type of large outdoor performance space. However, in addition to the acoustic descriptors related to aural perception defined in ISO 3382-1, this study has highlighted the importance of analyzing the acoustic signature of the place, which provides early reflections of the impulse response. Through the frequency response (RFR) and the spatiotemporal analysis of the intensity hedgehogs in the Ronda bullring, the diffraction of sound caused by the rows of seats has also been verified in a similar way to that which occurs in the stands of classical theatres.

It has been shown that the majority of evaluated acoustic descriptors maintain values within the typical ranges for use as a performance space and their frequency dependence is satisfactory. However, the great variability in the EDT parameter provides a warning for this parameter to be utilized with extreme care. Although musical clarity and definition are related, it is preferable to use D_{50} so that any issues that may arise when late energy is very small or absent can be avoided. The virtual acoustic techniques utilized herein have enabled the reconstruction of the sound field of the Ronda bullring and the comparison of the influence of the presence of the public depending on the degree of occupancy, together with the variations due to the location of the various sound sources.

Author Contributions: Conceptualization, M.M.-C., S.G. and M.G.; methodology, M.M.-C., S.G. and M.G.; software, M.M.-C.; validation, M.M.-C.; investigation, M.M.-C.; resources, M.M.-C., S.G. and M.G.; writing—original draft preparation, M.M.-C.; writing—review and editing, S.G. and M.G.; supervision, S.G. and M.G. All authors have read and agreed to the published version of the manuscript.

Funding: The translation of the paper has been financed by the IUACC 2023 Research Internationalization Grants from the VII Own Research and Transfer Plan of the University of Seville.

Data Availability Statement: The data presented in this study is available on request from the corresponding authors. The data is not publicly available due to privacy.

Acknowledgments: The authors wish to express their gratitude to the management of the Real Maestranza de Caballería de Ronda and to all the staff of its bullring who so kindly assisted during the measurement campaign. Special thanks go to the architects of the bullring for the graphic documentation provided and to F. J. Nieves, J. Alayón and the INTROMAC (Instituto Tecnológico de Rocas Ornamentales y Materiales de Construcción) for their collaboration in the field acoustic measurements.

Conflicts of Interest: The authors declare there to be no conflicts of interest.

Appendix A

Table A1. Comparison of averaged grid simulated results at each octave band, without the audience (first row) and with the audience (second row) for the various acoustic parameters and for S1, S2, S3, and S4 sound sources.

	Frequency [kHz]						**Frequency [kHz]**					
	0.125	**0.25**	**0.5**	**1**	**2**	**4**	**0.125**	**0.25**	**0.5**	**1**	**2**	**4**
	T_{30} [s]						EDT [s]					
S1	2.57	2.21	2.02	1.98	1.83	1.55	2.53	2.38	2.37	2.31	2.29	2.26
	1.80	1.47	1.30	1.26	1.20	1.12	2.29	2.55	2.71	2.62	2.56	2.45
S2	2.61	2.29	2.10	2.06	1.91	1.65	2.04	1.62	1.44	1.42	1.31	1.13
	1.95	1.65	1.49	1.45	1.39	1.29	1.40	1.15	1.06	1.04	0.99	0.87
S3	2.60	2.25	2.08	2.04	1.92	1.68	2.41	2.04	1.87	1.83	1.70	1.44
	1.90	1.60	1.47	1.44	1.39	1.30	1.82	1.59	1.46	1.41	1.32	1.08
S4	2.58	2.23	2.06	2.01	1.88	1.65	2.41	2.02	1.85	1.79	1.65	1.39
	1.93	1.64	1.51	1.48	1.43	1.33	1.73	1.41	1.25	1.19	1.12	0.99
	C_{80} [dB]						D_{50}					
S1	0.5	0.5	0.5	0.5	0.6	0.6	0.06	0.05	0.05	0.04	0.04	0.04
	0.6	0.6	0.6	0.6	0.6	0.7	0.05	0.04	0.03	0.03	0.03	0.03
S2	0.5	0.6	0.6	0.6	0.6	0.6	0.15	0.15	0.16	0.16	0.16	0.17
	0.6	0.7	0.6	0.7	0.7	0.7	0.14	0.14	0.14	0.14	0.15	0.15
S3	0.4	0.4	0.5	0.5	0.5	0.5	0.16	0.15	0.15	0.15	0.15	0.15
	0.6	0.7	0.7	0.7	0.7	0.7	0.14	0.13	0.13	0.13	0.13	0.14
S4	0.4	0.5	0.5	0.5	0.5	0.6	0.15	0.15	0.15	0.15	0.15	0.15
	0.6	0.7	0.7	0.7	0.7	0.7	0.14	0.14	0.14	0.14	0.14	0.14
	J_{LF}						L_J [dB]					
S1	0.06	0.05	0.05	0.04	0.04	0.04	−7.4	−9.4	−10.4	−10.6	−11.3	−12.5
	0.05	0.04	0.03	0.03	0.03	0.03	−9.9	−12.3	−13.5	−13.8	−14.3	−15.1
S2	0.15	0.15	0.16	0.16	0.16	0.17	−6.9	−8.6	−9.5	−9.6	−10.2	−11.4
	0.14	0.14	0.14	0.14	0.15	0.15	−9.2	−11.2	−12.1	−12.4	−12.7	−13.6
S3	0.16	0.15	0.15	0.15	0.15	0.15	−7.1	−8.5	−9.2	−9.4	−10.2	−11.8
	0.14	0.13	0.13	0.13	0.13	0.14	−13.1	−15.6	−16.9	−17.3	−17.6	−18.4
S4	0.15	0.15	0.15	0.15	0.15	0.15	−7.3	−8.7	−9.6	−9.8	−10.5	−12.1
	0.14	0.14	0.14	0.14	0.14	0.14	−12.2	−14.5	−15.9	−16.3	−16.6	−17.4
	G [dB]									STI		
S1	1.6	0.6	0.2	0.2	−0.1	−0.6				0.57		
	0.7	−0.3	−0.7	−0.7	−0.9	−1.3				0.61		
S2	1.8	0.7	0.3	0.1	−0.2	−0.8				0.58		
	0.8	−0.2	−0.7	−0.9	−1.1	−1.5				0.64		
S3	0.5	−0.5	−0.9	−1.0	−1.6	−2.5				0.52		
	−3.7	−5.2	−6.1	−6.2	−6.4	−6.7				0.63		
S4	0.5	−0.5	−1.1	−1.1	−1.6	−2.4				0.53		
	−2.6	−4.0	−4.8	−4.9	−5.1	−5.4				0.63		

References

1. Diaz-Recasens, G.; Vázquez-Consuegra, G. *Las Plazas de Toros (The Bullrings)*, 4th ed.; Dirección General de Arquitectura y Vivienda. Consejería de Obras Públicas y Transportes: Sevilla, Spain, 2004.
2. Martín-Castizo, M.; Girón, S.; Galindo, M. A proposal for the acoustic characterization of circular bullrings. *J. Acoust. Soc. Am.* **2022**, *152*, 380–398. [CrossRef]

3. Blesser, B.; Salter, L.R. *Spaces Speak, Are You Listening? Experiencing Aural Architecture*, 1st ed.; The MIT Press: Cambridge, MA, USA, 2009.
4. UNESCO. Text of the Convention for the Safeguarding of the Intangible Cultural Heritage 2003. Available online: https://ich.unesco.org/en/convention (accessed on 5 October 2023).
5. UNESCO. General Conference, 39th 2017. The Importance of Sound in Today's World: Promoting Best Practices 2017. Available online: https://unesdoc.unesco.org/ark:/48223/pf0000259172 (accessed on 5 October 2023).
6. Kolar, M.A. Archaeoacoustics: Re-sounding material culture. *Acoust. Today* **2018**, *14*, 28–37. [CrossRef]
7. Jahn, R.G.; Devereux, P.; Ibison, M. Acoustical resonances of assorted ancient structures. *J. Acoust. Soc. Am.* **1996**, *99*, 649–658. [CrossRef]
8. Scarre, C.; Lawson, G. (Eds.) *Archaeoacoustics*, 1st ed.; McDonald Institute for Archaeological Research University of Cambridge: Cambridge, UK, 2006.
9. Brezina, P. Acoustics of historic spaces as a form of intangible cultural heritage. *Antiquity* **2013**, *87*, 574–580. [CrossRef]
10. Till, R. Sound archaeology: A study of the acoustics of three world heritage sites, Spanish prehistoric painted caves, Stonehenge, and Paphos theatre. *Acoustics* **2019**, *21*, 661–692. [CrossRef]
11. Katz, B.F.G.; Murphy, D.; Farina, A. The past has ears (PHE): XR Explorations of acoustic spaces as cultural heritage. In Proceedings of the International Conference on Augmented Reality, Virtual Reality and Computer Graphics AVR, Salento, Italy, 8–11 June 2020; pp. 91–98.
12. Gerzon, M.A. Recording concert hall acoustics for posterity. *J. Audio Eng. Soc.* **1975**, *23*, 569–571.
13. Yamasaki, Y.; Itow, T. Measurement of spatial information in sound fields by closely located four point microphone method. *J. Acoust. Soc. Japan* **1989**, *10*, 101–110. [CrossRef]
14. Abdou, A.; Guy, R.W. Spatial information of sound fields for room-acoustics evaluation and diagnosis. *J. Acoust. Soc. Am.* **1996**, *100*, 3215–3226. [CrossRef]
15. Farina, A.; Tronchin, L. 3D Impulse response measurements on S. Maria del Fiore Church, Florence, Italy. *J. Acoust. Soc. Am.* **1998**, *103*, 3034. [CrossRef]
16. Merimaa, J.; Lokki, T.; Peltonen, T.; Karjalainen, M. Measurement, analysis, and visualization of directional room responses. In Proceedings of the 111th Audio Engineering Society (AES) Convention, New York, NY, USA, 21–24 September 2001; pp. 1–9.
17. Fukushima, Y.; Suzuki, H.; Omoto, A. Visualization of reflected sound in enclosed space by sound intensity measurement. *Acoust. Sci. Tech.* **2006**, *27*, 187–189. [CrossRef]
18. Martellotta, F. On the use of microphone arrays to visualize spatial sound field information. *Appl. Acoust.* **2013**, *74*, 987–1000. [CrossRef]
19. Pätynen, J.; Tervo, S.; Lokki, T. Analysis of concert hall acoustics via visualizations of time-frequency and spatiotemporal responses. *J. Acoust. Soc. Am.* **2013**, *133*, 842–857. [CrossRef] [PubMed]
20. Beranek, L.L. *Concert and Opera Halls: How They Sound*, 1st ed.; American Institute of Physics: New York, NY, USA, 1996.
21. Gómez, J.O.G.; Wright, O.; Van Den Braak, B.; Sanz, J.; Kemp, L.; Hulland, T. On the sequence of unmasked reflections in shoebox concert halls. *Appl. Sci.* **2021**, *11*, 7798. [CrossRef]
22. Lokki, T.; Pätynen, J.; Tervo, S.; Siltanen, S.; Savioja, L. Engaging concert hall acoustics is made up of temporal envelope preserving reflections. *J. Acoust. Soc. Am.* **2011**, *129*, EL223–EL228. [CrossRef]
23. Vorländer, M. *Auralization. Fundamentals of Acoustics, Modelling, Simulation, Algorithms and Acoustic Virtual Reality*, 1st ed.; Springer: Berlin, Germany, 2008.
24. Savioja, L.; Xiang, N. Introduction to the special issue on room acoustic modeling and auralization. *J. Acoust. Soc. Am.* **2019**, *145*, 2597–2600. [CrossRef] [PubMed]
25. Krokstad, A.; Svensson, U.P.; Strøm, S. The early history of ray tracing in acoustics BT—Acoustics, information, and communication. In *Memorial Volume in Honor of Manfred R. Schroeder*, 1st ed.; Xiang, N., Sessler, G.M., Eds.; Springer: New York, NY, USA, 2015; pp. 15–31.
26. Savioja, L.; Svensson, U.P. Overview of geometrical room acoustic modeling techniques. *J. Acoust. Soc. Am.* **2015**, *138*, 708–730. [CrossRef] [PubMed]
27. Fratoni, G.; Hamilton, B.; D'Orazio, D. Feasibility of a finite-difference time-domain model in large-scale acoustic simulations. *J. Acoust. Soc. Am.* **2022**, *152*, 330–341. [CrossRef]
28. Suárez, R.; Alonso, A.; Sendra, J.J. Intangible cultural heritage: The sound of the Romanesque cathedral of Santiago de Compostela. *J. Cult. Herit.* **2015**, *16*, 239–243. [CrossRef]
29. De Muynke, J.; Baltazar, M.; Monferran, M.; Voisenat, C.; Katz, B.F. Ears of the past, an inquiry into the sonic memory of the acoustics of Notre-Dame before the fire of 2019. *J. Cult. Herit.* **2022**, *in press*. [CrossRef]
30. D'Orazio, D.; Fratoni, G.; Rovigatti, A.; Garai, M. A virtual orchestra to qualify the acoustics of historical opera houses. *Build. Acoust.* **2020**, *27*, 235–252. [CrossRef]
31. Postma, B.N.; Dubouilh, S.; Katz, B.F. An archeoacoustic study of the history of the Palais du Trocadero (1878–1937). *J. Acoust. Soc. Am.* **2019**, *145*, 2810–2821. [CrossRef]

32. Sü Gül, Z. Exploration of room acoustics coupling in Hagia Sophia of Istanbul for its different states. *J. Acoust. Soc. Am.* **2021**, *149*, 320–339. [CrossRef]
33. Pilch, A. Optimization-based method for the calibration of geometrical acoustic models. *Appl. Acoust.* **2020**, *170*, 107495. [CrossRef]
34. Vorländer, M. Computer simulations in room acoustics: Concepts and uncertainties. *J. Acoust. Soc. Am.* **2013**, *133*, 1203–1213. [CrossRef]
35. Rindel, J.H. A note on modal reverberation times in rectangular rooms. *Acta Acust. United Acust.* **2016**, *102*, 9600–9603. [CrossRef]
36. Christensen, C.L.; Nielsen, G.B.; Rindel, J.H. Danish Acoustical Society Round Robin on Room Acoustic Computer Modelling. 2008. Available online: https://odeon.dk/product/reliability-tests/?hilite=Danish+Acoustical+Society+Round+Robin+room+acoustic+computer+modelling (accessed on 8 December 2023).
37. Real Maestranza de Caballería de Ronda. Available online: https://www.rmcr.org/ (accessed on 8 December 2023).
38. Garrido, F.; Garrido, A. *II Centenario de la Plaza de Toros de la Real Maestranza de Caballería de Ronda 1785–1085*, 1st ed.; Real Maestranza de Ronda: Ronda, Spain, 1988.
39. Romero-Solís, P. Plaza de Toros de Ronda 225 años. *Rev. Estud. Taur.* **2011**, *29*, 275–278.
40. Arquitectura de la Plaza de Toros de Ronda. Plaza y Museo RMR. 2018. Available online: https://plazaymuseormr.wordpress.com/2018/10/05/arquitectura-de-la-plaza-de-toros-de-ronda/ (accessed on 8 December 2023).
41. Miró-Domínguez, A. La plaza de toros de Ronda. *Jábega* **1985**, *50*, 165–181.
42. SketchUp. Available online: https://www.sketchup.com/ (accessed on 8 December 2023).
43. Borreroycaballos.com. Available online: https://borreroycaballos.com/restauracion-real-maestranza-caballeria-ronda/ (accessed on 8 December 2023).
44. ODEON Room Acoustics Software. Technical University of Denmark. Available online: https://www.odeon.dk/ (accessed on 8 December 2023).
45. *ISO 3382-1*; Acoustics–Measurements of Room Acoustic Parameters. Part I: Performance Rooms. ISO: Geneva, Switzerland, 2009.
46. *ISO 3382-2*; Acoustics–Measurement of Room Acoustic Parameters. Part 2: Reverberation Time in Ordinary Rooms. ISO: Geneva, Switzerland, 2008.
47. Tronchin, L. Variability of room acoustic parameters with thermo-hygrometric conditions. *Appl. Acoust.* **2021**, *177*, 107933. [CrossRef]
48. IRIS 3D Measurement System, IRIS 1.2 User Manual 2018. Available online: https://www.iris.co.nz/ (accessed on 8 December 2023).
49. Girón, S.; Galindo, M.; Romero-Odero, J.A.; Alayón, J.; Nieves, F.J. Acoustic ambience of two Roman theatres in the Cartaginensis province of Hispania. *Build. Environ.* **2021**, *193*, 107653. [CrossRef]
50. PTB (Physikalisch Technische Bundesanstalt). The Room Acoustics Absorption Coefficient Database 2012. Available online: https://www.ptb.de/cms/ptb/fachabteilungen/abt1/fb-16/ag-163/absorption-coefficient-database.html (accessed on 8 December 2023).
51. Martellotta, F. On the sound absorption by openings in rooms. *J. Acoust. Soc. Am.* **2012**, *132*, 2951–2954. [CrossRef]
52. Harris, C.M.; Piersol, A.G. *Harris' Shock and Vibration Handbook*, 5th ed.; McGraw-Hill: New York, NY, USA, 2002.
53. Yang, H.S. Outdoor Noise Control by Natural/Sustainable Materials in Urban Areas. Ph.D. Dissertation, University of Sheffield, Sheffield, UK, 2013.
54. *IEC 60268-16*; Sound System Equipment–Part 16: Objective Rating of Speech Intelligibility by Speech Transmission Index. IEC: Geneva, Switzerland, 2020.
55. Rindel, J.H. A note on meaningful acoustical parameters for open-air theatres. *Acta Acust. United Acust.* **2023**, *7*, 20. [CrossRef]
56. Gade, A. Acoustics in halls for speech and music. In *Springer Handbook of Acoustics*, 1st ed.; Rossing, T.D., Ed.; Springer: New York, NY, USA, 2007; pp. 301–350.
57. Girón, S.; Álvarez-Corbacho, A.; Zamarreño, T. Exploring the acoustics of ancient open-air theatres. *Arch. Acoust.* **2020**, *45*, 181–208.
58. Cabrera, D.; Lee, D.; Leembruggen, G.; Jimenez, D. Increasing robustness in the calculation of the speech transmission index from impulse responses. *Build. Acoust.* **2014**, *21*, 181–198. [CrossRef]
59. Vassilantonopoulos, S.; Hatziantoniou, P.; Tatlas, N.-A.; Zakynthinos, T.; Skarlatos, D.; Mourjopoulos, J.N. Measurements and analysis of the acoustics of the ancient theater of Epidauros. In Proceedings of the Acoustics of Ancient Theatres Conference, Patras, Greece, 18–21 September 2011; pp. 1–9.
60. Economou, P.; Charalampous, P.; Ioannides, S.; Polykarpou, P. The significance of sound diffraction effects in simulating acoustics in ancient theatres. In Proceedings of the Acoustics of Ancient Theatres Conference, Patras, Greece, 18–21 September 2011; pp. 1–14.
61. Lokki, T.; Southern, A.; Siltanen, S.; Savioja, L. Acoustics of Epidaurus—Studies with room acoustics modelling methods. *Acta Acust. United Acust.* **2013**, *99*, 40–47. [CrossRef]
62. Bradley, J.S. Review of objective room acoustics measures and future needs. *Appl. Acoust.* **2011**, *72*, 713–720. [CrossRef]

63. Larrosa-Navarro, M.; De La Prida, D.; Pedrero, A. Influence of musical stimulus on the perception of clarity in rooms and its relation to C80. *Appl. Acoust.* **2023**, *208*, 109370. [CrossRef]
64. Solar-Dorrego, F.; Vigeant, M.C. A study of the just noticeable difference of early decay time for symphonic halls. *J. Acoust. Soc. Am.* **2022**, *151*, 80–94. [CrossRef]